Physical Review B 58, 4672 (1998)

Canted antiferromagnetic and spin singlet quantum Hall states in double-layer systems

S. Das Sarma[1], Subir Sachdev[2], and Lian Zheng[1]

[1]*Department of Physics, University of Maryland, College Park, Maryland 20742-4111*

[2]*Department of Physics, Yale University, P.O. Box 208120, New Haven, CT 06520-8120*

(June 28, 2000)

Abstract

We present details of earlier studies (Zheng *et al*, Phys. Rev. Lett. **78**, 310 (1997) and Das Sarma *et al*, *ibid* **79**, 917 (1997)) and additional new results on double-layer quantum Hall systems at a total filling $\nu = 2\nu_1$, where a single layer at filling ν_1 forms a ferromagnetic, fully spin-polarized, gapped incompressible quantum Hall state. For the case $\nu_1 = 1$, a detailed Hartree-Fock analysis is carried out on a realistic, microscopic Hamiltonian. Apart from the state continuously connected to the ground state of two well separated layers, we find two double-layer quantum Hall phases: one with a finite interlayer antiferromagnetic spin ordering in the plane orthogonal to the applied field (the 'canted' state), and the other a spin singlet. The quantum transitions between the various quantum Hall states are continuous, and are signaled by the softening of collective intersubband spin density excitations. For the case of general ν_1, closely related results are obtained by a semi-phenomenological continuum quantum field theory description of the low-lying spin excitations using a non-linear sigma model. Because of its broken symmetry, the canted phase supports a linearly dispersing Goldstone mode and has a finite temperature Kosterlitz-Thouless transition. We present results on the form of the phase diagram, the magnitude of the canted order parameter, the collective

excitation dispersions, the specific heat, the form of the dynamic light scattering spectrum at finite temperature, and the Kosterlitz-Thouless critical temperature. Our findings are consistent with recent experimental results.
73.40.Hm 73.20.Mf 73.20.Dx

I. INTRODUCTION

Interaction in a low-dimensional system does not merely result in strong renormalization of physical quantities, but can in many cases drive the system into completely new phases with peculiar properties. For a two-dimensional (2D) electron gas in a perpendicular magnetic field, the interaction effects are especially important because of Landau level quantization. When electrons are entirely restricted to the lowest Landau level by a large magnetic field, electron-electron interaction completely dominates the properties of the system as the electron kinetic energy is quenched to an unimportant constant. One of the most interesting phenomena in this strongly-correlated system is the quantum Hall (QH) effect, which has attracted a great deal of experimental and theoretical interest during the last fifteen years[1]. Recent advances in materials growth techniques have made it possible to fabricate high-quality double-layer two-dimensional electron systems with the electrons confined to two parallel planes separated by a distance comparable to that between electrons within a plane. With the introduction of this layer degree of freedom, many qualitatively new effects due entirely to interlayer correlations appear[2–9]. Many new QH phases in double-layer systems become real possibilities because of the increased degree of freedom and the complicated interplay among interlayer tunneling energy, Zeeman energy, and electron-electron Coulomb interaction energy.

In this paper, we present the details of our earlier theoretical investigations[7,9] of the possible QH phases in a double-layer system at a *total* Landau level filling factor $\nu = 2\nu_1$, where ν_1 is a filling factor at which an isolated single layer system forms a fully spin polarized incompressible QH state (*e.g.* $\nu_1 = 1,\ 1/3$, *etc.*) We will discuss three distinct ground states, and the nature of the zero or finite temperature transitions/crossovers between them:

- A fully polarized ferromagnetic (FPF) QH state in which the spins in each layer are aligned parallel to the magnetic field. This state is adiabatically connected to the ground state of well separated layers, each forming a polarized QH state at filling fraction ν_1. We will denote this FPF state also as the FM (for "ferromagnetic") state.

- A spin singlet (SS) state, which can be visualized crudely as consisting of singlet pairs of electrons in opposite layers. Alternatively, at $\nu_1 = 1$, we will discuss the Hartree-Fock picture of spin up and spin down electrons fully occupying single-particle states which are symmetric in the layer "pseudospin" index; hence the singlet state will also be referred to as SYM. In the limit of a vanishing tunneling matrix element between the layers, this state is simply the pseudospin polarized state of Refs 3,4 for both spin up and spin down electrons separately. Throughout, we will consider the case of a non-vanishing tunneling matrix element: in this case the pseudospin polarization is chosen by the phase of the tunneling amplitude, and not spontaneously. None of the phase transitions we consider here require a vanishing tunneling matrix element; on the contrary, changes in the value of the tunneling matrix element can drive the quantum transitions.

- A canted state (C) in which the average spin moments in the layers have an antiferromagnetic correlation in the plane perpendicular to the magnetic field, and a ferromagnetic correlation parallel to the magnetic field. Both ferromagnetic and antiferromagnetic moments can vary continuously at zero temperature as parameters are varied. The planar antiferromagnetic ordering breaks spin rotation symmetry about the magnetic field axis: as a consequence there is a gapless, linearly dispersing, Goldstone collective mode in its excitation spectrum and a Kosterlitz-Thouless transition at a finite temperature. The C phase is the canted antiferromagnetic phase (CAF) discussed in our earlier short publications[7,9].

We will use two distinct and complementary approaches to understand these phases. The first is a mean-field Hartree-Fock calculation: this applies only for integer values of ν_1, but has the advantage of working with a precise microscopic Hamiltonian involving only parameters which are directly known experimentally. The second is a phenomenological, quantum field-theoretic formulation which applies for general ν_1, and allows us to more precisely understand the consequences of thermal and quantum fluctuations. We will now

discuss some of the results of these two approaches in turn.

In the Hartree-Fock approximation[10], we are able to show that the canted antiferromagnetic (C) phase is the energetically favored ground state for $\nu = 2$ at intermediate layer separations for systems with small Zeeman energy, and that the phase transitions from the C to the FM or SYM phases are continuous. We evaluate at $\nu = 2$ the intersubband spin density wave (SDW) dispersions of all phases in the time-dependent Hartree-Fock approximation[11] and show that, as the precursor of the phase transitions, the collective intersubband SDW mode softens at the phase boundaries of the FM and SYM phases to the C phase. The SDW becomes the linearly dispersing Goldstone mode in the C phase, and the temperature of the Kosterlitz-Thouless transition is obtained by evaluating its effective spin-stiffness in the Hartree-Fock approximation. In addition we present results on the stability energetics of the various phases, the antiferromagnetic order parameter, the phase diagram, the collective intersubband SDW excitation dispersions, and the specific heat.

The $\nu = 2$ Hartree-Fock results may also be qualitatively applicable to the case of $\nu = 6$ if the Landau level mixing is ignored (the Landau level mixing may not be negligible at $\nu = 6$, though.) On the other hand, the situation at $\nu = 4$ is very different from the situation at $\nu = 2$, since the inter-Landau level excitation energies are comparable to the cyclotron energy; our results do not apply at $\nu = 4$.

The microscopic Hartree-Fock analysis obviously does not apply to a situation where the average filling factor ν_1 in each layer is fractional (e.g. $\nu_1 = 1/3$) with each isolated layer supporting a spin polarized Laughlin fractional QHE state; such a many-body state will not appear in any mean-field decoupling of the Hamiltonian. However, an essential property of the phases we are discussing is that they all have a gap towards charged excitations, and the transitions between them are driven by changes in the nature of the mean spin polarizations, and of the spin excitations. This suggests that it may be possible to develop a more general effective theory which focuses on the spin excitations alone. We will present such a theory in Section III: it turns out to be the $O(3)$ quantum non-linear sigma model in the presence of a magnetic field. For the case $\nu = 2$, we are able to use our earlier Hartree-

Fock computations to precisely obtain all the renormalized parameters which universally determine the low temperature properties of the non-linear sigma model; for other values of ν_1, including the fractional cases, these parameters remain as phenomenological inputs. We will present the phase diagram of the sigma model, and describe the nature of the finite temperature crossovers above the various phases in some details. In particular, we will obtain explicit predictions for the temperature dependence of the line shape of the inelastic light scattering spectrum.

We note that our findings from the two approaches are consistent with recent inelastic light scattering measurement[8], where a remarkable (and temperature dependent) softening of the long wavelength intersubband SDW mode in a $\nu = 2$ double-layer system is observed. We hope that our other explicit theoretical results may be tested in future experiments. The experimental situation will be discussed in Section IV.

This paper is organized as follows. The results of the Hartree-Fock theory are presented in Section II. In Section II A, we study the ground state properties of the $\nu = 2$ double-layer system in a self-consistent mean-field approximation. The intersubband SDW excitations in the time-dependent Hartree-Fock approximation and associated mode softening are studied in Section II B. The thermodynamic properties are discussed in Section II C, and some further discussion, along with an assessment of the validity of the calculation, appear in Sections II D and II E. In a long and self-contained Section III we give our non-linear σ model effective field theoretic description for a generic $\nu = 2\nu_1$ situation. Comparison of our theory with recent light scattering experiments is discussed in section IV. A short summary in section V concludes this paper. We note that the readers who are interested only in microscopic Hartree-Fock theory could skip Section III, and the readers who are interested only in our long wavelength effective field theory could skip Section II. We have taken care in writing the two parts of our work, namely the microscopic Hartree-Fock calculation for $\nu = 2$ (Section II) and the non-linear σ model description for $\nu = 2\nu_1$ (Section III) as two separate self-contained pieces which can be read reasonably independent of each other if so desired.

II. HARTREE-FOCK THEORY

We begin by writing down the explicit microscopic Hamiltonian of a double layer quantum Hall system.

Within the lowest Landau level, the single particle eigenstates may be denoted by $|\alpha\mu\sigma\rangle$, where α is the intra-Landau-level index in the lowest Landau level, $\mu = 0, 1$ is the pseudospin index which labels the symmetric and antisymmetric subbands, and the spin index $\sigma = \pm 1$ labels $\uparrow$ and $\downarrow$ spins.[16] The Hamiltonian of the double-layer system is

$$H = H_0 + H_{\rm I}, \tag{2.1}$$

where the non-interacting Hamiltonian is

$$H_0 = -\Delta_{\rm sas} \sum_{\alpha\mu\sigma} (1/2 - \mu) C^\dagger_{\alpha\mu\sigma} C_{\alpha\mu\sigma} - \Delta_z \sum_{\alpha\mu\sigma} \frac{\sigma}{2} C^\dagger_{\alpha\mu\sigma} C_{\alpha\mu\sigma}, \tag{2.2}$$

where the pseudospin splitting $\Delta_{\rm sas}$ is the tunneling-induced symmetric-antisymmetric energy separation, the spin splitting Δ_z is the Zeeman energy, and $C^\dagger$ (C) is electron creation (annihilation) operator. The Coulomb interaction Hamiltonian $H_{\rm I}$ is

$$\begin{aligned} H_{\rm I} = \frac{1}{2} \sum_{\sigma_1\sigma_2} \sum_{\mu_1\mu_2\mu_3\mu_4} \sum_{\alpha_1\alpha_2} \frac{1}{\Omega} \sum_{\mathbf{q}} V_{\mu_1\mu_2\mu_3\mu_4}(q) e^{-q^2 l_o^2/2} e^{iq_x(\alpha_1-\alpha_2)l_o^2} \\ \times C^\dagger_{\alpha_1+q_y\mu_1\sigma_1} C^\dagger_{\alpha_2\mu_2\sigma_2} C_{\alpha_2+q_y\mu_3\sigma_2} C_{\alpha_1\mu_4\sigma_1}, \end{aligned} \tag{2.3}$$

where Ω is the area of the system, $l_o = (\hbar c/eB)^{1/2}$ is the magnetic length. The non-zero Coulomb potential matrix elements are $V_{0000} = V_{0110} = V_{1001} = V_{1111} = V_+$ and $V_{1010} = V_{0101} = V_{1100} = V_{0011} = V_-$, with $V_\pm(q) = \frac{1}{2}[v_a(q) \pm v_b(q)]$, where $v_a(q) = \frac{2\pi e^2}{\epsilon q}$ and $v_b(q) = v_a(q)e^{-qd}$ are the intralayer and interlayer Coulomb interaction potentials, respectively. (The finite well-thickness corrections can be taken into consideration by including appropriate form factors[10].)

The following subsections will examine various properties of H at $\nu = 2$ by mean-field and RPA-like treatments of the interactions in $H_{\rm I}$.

A. Ground states

In this subsection, we investigate the ground state properties of H, and obtain the three phases discussed in the Introduction. Performing Hartree-Fock pairing of (2.3), one obtains the mean-field interaction Hamiltonian as

$$H_{\rm I}^{\rm HF} = -\sum_{\sigma_1\sigma_2}\sum_{\mu_1\mu_2} X_{\mu_1\mu_2\sigma_1\sigma_2} C^\dagger_{\mu_1\sigma_1} C_{\mu_2\sigma_2}, \tag{2.4}$$

where $X_{\mu_1\mu_2\sigma_1\sigma_2} = \frac{1}{2\pi l_o^2}\sum_{\mu_3\mu_4}\sum_{\mathbf{q}} V_{\mu_3\mu_1\mu_4\mu_2}(q) e^{-q^2 l_o^2/2} < C^\dagger_{\mu_3\sigma_2} C_{\mu_4\sigma_1} >$, which depends on the electronic state being sought through the expectation value $< C^\dagger_{\mu_3\sigma_2} C_{\mu_4\sigma_1} >$. We self-consistently search for the symmetry broken states where, in addition to $< C^\dagger_{\mu\sigma} C_{\mu\sigma} > \neq 0$, the possibility that $< C^\dagger_{\mu\uparrow} C_{1-\mu\downarrow} > \neq 0$ is also allowed. Because of the complete Landau level degeneracy, the Hartree-Fock Hamiltonian $H^{\rm HF} = H_0 + H_{\rm I}^{\rm HF}$ in a uniform state is a 4×4 matrix, representing the dimension of the subspace associated with the spin and layer degrees of freedom. It thus has four eigenenergies $\varepsilon_{i\pm}$ and four eigenstates $\phi_{i\pm}$ $(i = 1, 2)$, which are obtained as shown below. In the non-interacting base $(|0\uparrow\rangle, |1\downarrow\rangle, |0\downarrow\rangle, |1\uparrow\rangle)$, $H^{\rm HF}$ becomes

$$H^{\rm HF} = \begin{pmatrix} E_1 & \Delta_1 & 0 & 0 \\ \Delta_1 & E_2 & 0 & 0 \\ 0 & 0 & E_3 & \Delta_2 \\ 0 & 0 & \Delta_2 & E_4 \end{pmatrix}, \tag{2.5}$$

where

$$\begin{aligned} E_1 &= -\frac{\Delta_{\rm sas}+\Delta_z}{2} - U_+(n_{1+}\sin^2\frac{\theta_1}{2} + n_{1-}\cos^2\frac{\theta_1}{2}) \\ &\quad -U_-(n_{2+}\cos^2\frac{\theta_2}{2} + n_{2-}\sin^2\frac{\theta_2}{2}), \\ E_2 &= \frac{\Delta_{\rm sas}+\Delta_z}{2} - U_+(n_{1+}\cos^2\frac{\theta_1}{2} + n_{1-}\sin^2\frac{\theta_1}{2}) \\ &\quad -U_-(n_{2+}\sin^2\frac{\theta_2}{2} + n_{2-}\cos^2\frac{\theta_2}{2}), \\ E_3 &= \frac{\Delta_z-\Delta_{\rm sas}}{2} - U_+(n_{2+}\sin^2\frac{\theta_2}{2} + n_{2-}\cos^2\frac{\theta_2}{2}) \end{aligned}$$

$$
\begin{aligned}
&-U_-(n_{1+}\cos^2\frac{\theta_1}{2}+n_{1-}\sin^2\frac{\theta_1}{2}),\\
E_4 &= \frac{\Delta_{\rm sas}-\Delta_z}{2}-U_+(n_{2+}\cos^2\frac{\theta_2}{2}+n_{2-}\sin^2\frac{\theta_2}{2})\\
&-U_-(n_{1+}\sin^2\frac{\theta_1}{2}+n_{1-}\cos^2\frac{\theta_1}{2}),\\
\Delta_1 &= U_+\frac{n_{1-}-n_{1+}}{2}\sin\theta_1+U_-\frac{n_{2-}-n_{2+}}{2}\sin\theta_2,\\
\Delta_2 &= U_+\frac{n_{2-}-n_{2+}}{2}\sin\theta_2+U_-\frac{n_{1-}-n_{1+}}{2}\sin\theta_1.
\end{aligned}
\tag{2.6}
$$

where θ_1 and θ_2 are associated with the Hartree-Fock eigenstates $\phi_{i\pm}$ which need to be obtained self-consistently, $n_{i\pm}$ are electron occupation numbers $\langle\phi^\dagger_{i\pm}\phi_{i\pm}\rangle$, and $U_\pm = \frac{1}{\Omega}\sum_{\mathbf{p}} e^{-p^2l_o^2/2}V_\pm(p)$. The off-diagonal matrix elements Δ_i represent the possibility of the broken symmetry ($\langle C^\dagger_{\mu\uparrow}C_{1-\mu\downarrow}\rangle \neq 0$) mentioned above. By diagonalizing the Hartree-Fock Hamiltonian $H^{\rm HF}$ of Eq. (2.5), one obtains the eigenstates

$$
(\phi_{1+},\phi_{1-},\phi_{2+},\phi_{2-}) = \begin{pmatrix}
\sin(\theta_1/2) & \cos(\theta_1/2) & 0 & 0\\
\cos(\theta_1/2) & -\sin(\theta_1/2) & 0 & 0\\
0 & 0 & \sin(\theta_2/2) & \cos(\theta_2/2)\\
0 & 0 & \cos(\theta_2/2) & -\sin(\theta_2/2)
\end{pmatrix},
\tag{2.7}
$$

and the eigenenergies

$$
\begin{aligned}
\varepsilon_{1\pm} &= \frac{E_1+E_2}{2}\pm\sqrt{\frac{(E_1-E_2)^2}{4}+\Delta_1^2},\\
\varepsilon_{2\pm} &= \frac{E_3+E_4}{2}\pm\sqrt{\frac{(E_3-E_4)^2}{4}+\Delta_2^2}.
\end{aligned}
\tag{2.8}
$$

Eqns. (2.5) to (2.8) form the complete self-consistent Hartree-Fock equations which need to be solved numerically. In fact, the only quantities to be determined in this self-consistent manner are the two parameters θ_1 and θ_2, which, in turn, uniquely define the eigenstates through Eq. (2.7). The eigenenergies always satisfy $\varepsilon_{i-} < \varepsilon_{j+}$ $(i,j=1,2)$, so the ground state at $\nu = 2$ is given by $|\rangle = \Pi_i\phi^\dagger_{i-}|{\rm v}\rangle$, where $|{\rm v}\rangle$ is the vacuum state. The ground state energy is given by $E = \langle H_0 + \frac{1}{2}H_{\rm I}^{\rm HF}\rangle$.

There are several sets of θ_1 and θ_2 which make Eq. (2.7) the self-consistent solutions to the mean-field Hartree-Fock equations. One is $\theta_1 = 0$ and $\theta_2 = 0$, which corresponds

to the symmetric (SYM) state. Another is $\theta_1 = 0$ and $\theta_2 = \pi$, which corresponds to the spin polarized ferromagnetic (FM) state. These two are the spin-ferromagnets (FM) or layer pseudospin-'ferromagnets'[3,4] (SYM) whose existence is naturally expected in the presence of finite Zeeman and tunneling energies. More interesting is that, for $\Delta_{\rm sas} > \Delta_z$, there exists a solution at intermediate interlayer separations with $0 < \theta_i < \pi$. As we shall see shortly, this new state possesses a canted antiferromagnetic ordering (the C phase), *i.e.* an interlayer inplane antiferromagnetic spin ordering with the inplane spin magnetic moment in each layer being equal in magnitude and opposite of each other. The energies of these different states are shown in Fig.1. It is clear from this figure that the energetically favored ground state is the SYM state at small interlayer separations, the C state at intermediate separations, and the FM state at large interlayer separations. The $\nu = 2$ double-layer QH system thus undergoes two quantum phase transitions as the layer separation is increased from $d = 0$ to $d \to \infty$ at a fixed magnetic field.

To show the antiferromagnetic spin correlations, we rearrange the eigenstates as

$$\phi_{i\pm} = (1/\sqrt{2}\ )\left(|{\rm L}\rangle S^{\rm L}_{i\pm} + |{\rm R}\rangle S^{\rm R}_{i\pm}\right), \tag{2.9}$$

where $S^{L(R)}_{i\pm}$, electron spin configurations in the left (right) layer in the eigenstate $\phi_{i\pm}$, are $S^{\rm L}_{i-} = \cos(\theta_i/2)|\uparrow\rangle - \sin(\theta_i/2)|\downarrow\rangle$, $S^{\rm R}_{i-} = \cos(\theta_i/2)|\uparrow\rangle + \sin(\theta_i/2)|\downarrow\rangle$, and satisfy $(S^{\rm L}_{i+})^\dagger S^{\rm L}_{i-} = (S^{\rm R}_{i+})^\dagger S^{\rm R}_{i-} = 0$. We immediately obtain the canted antiferromagnetic spin order as

$$\langle \mathcal{S}^{\rm R}_x \rangle = -\langle \mathcal{S}^{\rm L}_x \rangle = \frac{1}{4}(\sin\theta_1 + \sin\theta_2), \tag{2.10}$$

where $\mathcal{S}^{L(R)}$ is the electron spin operator in the left (right) layer, and x denotes the spin alignment direction within the two dimensional plane. This canted interlayer antiferromagnetic spin ordering is shown schematically in Fig. 2. Note that the total spin magnetic moment still points in the direction of the magnetic field as required by symmetry. It is obvious that this antiferromagnetic order breaks the $U(1)$ symmetry associated with the spin-rotational invariance of the system. Its consequences on the low temperature thermodynamic properties will be discussed later. The numerical result of this order parameter

$|\langle \mathcal{S}_x^{\rm L}\rangle - \langle \mathcal{S}_x^{\rm R}\rangle|$ is shown in Fig.3. One can see that when Zeeman energy Δ_z is increased, the range of the layer separations where the canted antiferromagnetic state exists shrinks in favor of the ferromagnetic state, as the Zeeman energy obviously favors the spin polarized state. It is clear that the phase transition is continuous.

The phase diagram, shown in Fig. 4, can be constructed from this mean-field approximation. The states $|0\uparrow\rangle$ and $|1\uparrow\rangle$ are occupied in the FM phase, $|0\uparrow\rangle$ and $|0\downarrow\rangle$ are occupied in the SYM phase, and the C phase interpolates between them. The SYM phase exists for $\Delta_{\rm sas} > \Delta_z$ and $d < d_{c1}$, the C phase exists for $\Delta_{\rm sas} > \Delta_z$ and $d_{c1} < d < d_{c2}$, and the FM phase exists for either $\Delta_z > \Delta_{\rm sas}$ or $d > d_{c2}$. The FM phase is favored when Δ_z is increased, while the SYM phase is favored when $\Delta_{\rm sas}$ is increased. In the next subsection, the same phase diagram will be obtained by studying the softening of the intersubband SDW excitations in the time dependent Hartree-Fock approximation.

In this subsection we have studied the ground state properties of $\nu = 2$ double-layer QH systems in a mean-field Hartree-Fock approximation and showed the existence of three stable QH phases. The most interesting observation is the existence of a canted antiferromagnetic phase, with a broken spin rotation symmetry, in between the symmetric and the ferromagnetic phases.

B. Intersubband SDW excitations and mode softening

In this section, we study collective intersubband SDW spectrum of $\nu = 2$ double-layer QH systems in the time-dependent Hartree-Fock approximation.[11] These excitations involve flipping both spin and pseudospin of the electron and are the lowest energy excitations at $\nu = 2$. The phase instability is studied by investigating the softening of the collective intersubband SDW excitations. The results obtained in this section are in complete quantitative agreement with the results obtained from the ground state studies in the previous section, as, of course, they should be if the calculations are done correctly.

In the absence of interaction, the two branches of the intersubband SDW excitations

which correspond to transitions $|0\uparrow\rangle \leftrightarrow |1\downarrow\rangle$ and $|0\downarrow\rangle \leftrightarrow |1\uparrow\rangle$ have excitation energies $|\Delta_{\rm sas} \pm \Delta_z|$, where $\Delta_{\rm sas}$ and Δ_z are interlayer tunneling and Zeeman energies, respectively. Interaction renormalizes the excitation energies in two ways. One is a self-energy correction to the polarizability due to the loss of exchange energy when an electron is excited to a higher but empty level, which raises the excitation energies. The other is the vertex correction to the polarizability due to an excitonic attraction between the electron excited to the higher level and the hole it leaves behind, which lowers the excitation energies. In diagrammatic perturbation theories, the effect of the exchange energy on the excitation energies is accounted for by including the corresponding self-energy in electron Greens functions, and the effect of the excitonic attraction is represented by vertex corrections. The self-energy and the vertex correction must be consistent with each other obeying the Ward identity. The direct Hartree term does not influence the SDW excitations because Coulomb interaction is spin-rotationally invariant. Since the Coulomb interaction potentials are subband-index dependent, they may introduce mode-coupling between the two branches of the intersubband SDW excitations. This mode-coupling pushes down the frequency of the low-lying excitation and hence helps mode softening.

The intersubband SDW excitation spectra are obtained as the poles of the retarded intersubband spin-density response function

$$\chi^{\rm ret}(q,\omega) = -i\int_0^\infty e^{i\omega t}\langle[\rho_{SD}(\mathbf{q},t),\rho^\dagger_{SD}(-\mathbf{q},0)]\rangle, \tag{2.11}$$

where the intersubband SDW operator is defined as

$$\rho_{SD}(\mathbf{r}) = \sum_{i=1}^{2}\phi^\dagger_{i-}(\mathbf{r})\phi_{i+}(\mathbf{r}). \tag{2.12}$$

$\rho_{SD}(\mathbf{r})$ recovers to familiar forms $\rho_{SD}(\mathbf{r}) = \sum_\mu C^\dagger_{\mu\uparrow}(\mathbf{r})C_{1-\mu\downarrow}(\mathbf{r})$ in the spin polarized state ($\theta_1 = 0$ and $\theta_2 = \pi$), and $\rho_{SD}(\mathbf{r}) = \sum_\sigma C^\dagger_{0\sigma}(\mathbf{r})C_{1-\sigma}(\mathbf{r})$ in the symmetric state ($\theta_1 = \theta_2 = 0$).

$\chi^{\rm ret}(q,\omega)$ is evaluated in the time-dependent Hartree-Fock approximation,[11] which we adapt to double-layer systems and, for simplicity, we ignore all the higher Landau levels. As argued earlier, this should be a good approximation for our problem. In this approximation,

one includes the single-loop self-energy and the ladder vertex diagrams in the theory, which satisfies the Ward identities. This time-dependent Hartree-Fock approximation, therefore, corresponds to solving the vertex equation shown in Fig.5, where the electron propagators are the self-consistent Hartree-Fock Green's functions obtained from the mean-field approximation discussed in the previous section. Due to the fact that the Coulomb interaction is frequency independent and that the Landau levels are completely degenerate, the integral vertex equation can be transformed into an algebraic matrix equation.[11] The matrices can be further block diagonalized into 4×4 matrices, from which the poles of the spin-density response function can be (almost) analytically calculated.

Combining Eqns. (2.11) and (2.12), one obtains the spin density response function in the Matsubara frequencies[17]

$$\chi(q, i\omega) = e^{-q^2 l_o^2/2} \sum_{i\alpha} e^{-iq_x \alpha l_o^2} D_{i+}(i\omega) \Gamma_{i+}(q, i\omega, \alpha), \tag{2.13}$$

where

$$\begin{aligned} D_{i\lambda} &= \frac{1}{\beta} \sum_n \mathcal{G}_{i\lambda}(ip_n + i\omega) \mathcal{G}_{i-\lambda}(ip_n) \\ &= \frac{n_{i-\lambda} - n_{i\lambda}}{i\omega + \varepsilon_{i-\lambda} - \varepsilon_{i\lambda}} \\ &= \frac{1}{\lambda i\omega + \varepsilon_{i-} - \varepsilon_{i+}} \quad \text{for} \;\; T = 0, \end{aligned} \tag{2.14}$$

where $\beta = 1/k_B T$, $\mathcal{G}_{i\lambda}$ is the Green's function corresponding to the self-consistent Hartree-Fock eigenstate $\phi_{i\lambda}$ and eigenenergy $\varepsilon_{i\lambda}$ given in Eqns. (2.7) and (2.8), respectively. The ladder diagram vertex function is

$$\begin{aligned} \Gamma_{i\lambda}(q, i\omega, \alpha) = e^{iq_x \alpha l_o^2} - \frac{1}{\Omega} \sum_{p_x i' \alpha' \lambda'} & e^{-[p_x^2 + (\alpha - \alpha')^2] l_o^2/2} e^{ip_x q_y l_o^2} \\ & \times D_{i'\lambda'} \Gamma_{i'\lambda'}(q, i\omega, \alpha') \langle i\lambda; i' - \lambda' | V(p_x, \alpha - \alpha') | i - \lambda; i'\lambda' \rangle, \end{aligned} \tag{2.15}$$

where the interaction matrix element is

$$\begin{aligned} \langle i_1\lambda_1; i_2\lambda_2 | V(q) | i_3\lambda_3; i_4\lambda_4 \rangle = & \frac{1}{2} [1 + (-1)^{i_1 + i_2 + i_3 + i_4}] \left((S^L_{i_1\lambda_1})^\dagger S^L_{i_4\lambda_4} \right) \left((S^L_{i_2\lambda_2})^\dagger S^L_{i_3\lambda_3} \right) \\ & \times \left[V_+(q) \delta_{i_2 i_3} + V_-(q)(1 - \delta_{i_2 i_3}) \right], \end{aligned} \tag{2.16}$$

where $S^L_{i\lambda}$ is the electron spin states given in Eq. (2.9).

To solve the vertex equation, we perform the following Fourier transformations[11]

$$\overline{\Gamma}_{i\lambda}(k) = \sum_{\alpha} \Gamma_{i\lambda}(\alpha) e^{-ik\alpha l_o^2}, \tag{2.17}$$

and

$$\tilde{V}_{i\lambda;i'\lambda'}(\mathbf{q}) = \frac{1}{\Omega} \sum_{\mathbf{p}} e^{-p^2 l_o^2/2} e^{i\mathbf{p}\wedge\mathbf{q} l_o^2} V_{i\lambda;i'\lambda'}(\mathbf{p}), \tag{2.18}$$

where $\mathbf{p}\wedge\mathbf{q} = p_x q_y - p_y q_x$ and $V_{i\lambda;i'\lambda'} = \langle i\lambda; i' - \lambda' | V(q) | i - \lambda; i'\lambda' \rangle$, as given by Eq. (2.16). After an analytical continuation, one obtains

$$\chi^{\rm ret}(q,\omega) = e^{-q^2 l_o^2/2} \sum_{i=1,2} \Upsilon_{i+}(q,\omega), \tag{2.19}$$

where

$$\Upsilon = (D^{-1} + \tilde{V})^{-1} N, \tag{2.20}$$

N and Υ are 4×1 matrices, with $N_{i\lambda} = \Omega/2\pi l_o^2$, the number of magnetic flux passing through the system, and $\Upsilon_{i\lambda} = D_{i\lambda}(\omega)\overline{\Gamma}_{i\lambda}(q,\omega)$. D and $\tilde{V}$ are 4×4 matrices, with $D_{i\lambda;i'\lambda'} = \delta_{ii'}\delta_{\lambda\lambda'} D_{i\lambda}(\omega)$, and $\tilde{V}_{i\lambda;i'\lambda'}$ defined in Eq.. (2.18).

The intersubband SDW dispersion $\omega(q)$, which occurs as the pole of the retarded spin density response function $\chi^{\rm ret}$, is the solution to $\det|D^{-1}(\omega) + \tilde{V}(q,\omega)| = 0$. After a lengthy but straightforward algebraic manipulation, the two intersubband SDW dispersions $\omega_{\pm}(q)$ are obtained as

$$\begin{aligned} \omega_{\pm}^2 = {} & A^2 + B^2 - \tilde{V}_-^2 \cos(\theta_1 + \theta_2) \\ & \pm \sqrt{\left[\tilde{V}_- \left(1 - \cos(\theta_1+\theta_2)\right) A\right]^2 + 4B^2 (A+C)(A-C)}\ , \end{aligned} \tag{2.21}$$

where $A = \frac{1}{2}(a+b)$, $B = \frac{1}{2}(a-b)$, and $C = \frac{1}{2}\tilde{V}_- \left(1 + \cos(\theta_1+\theta_2)\right)$, with

$$\begin{aligned} a &= \sqrt{(\Delta_{\rm sas} + \Delta_z + U_+\cos\theta_1 - U_-\cos\theta_2)^2 + (U_+\sin\theta_1 + U_-\sin\theta_2)^2} - \tilde{V}_+, \\ b &= \sqrt{(\Delta_{\rm sas} - \Delta_z + U_+\cos\theta_2 - U_-\cos\theta_1)^2 + (U_+\sin\theta_2 + U_-\sin\theta_1)^2} - \tilde{V}_+. \end{aligned} \tag{2.22}$$

The intersubband SDW dispersions in both the canted antiferromagnetic QH phase (C) and the normal QH phases (FM or SYM) can be obtained from the above expression by incorporating appropriate values of θ_1 and θ_2. In the following, we show $\omega_\pm(q)$ only at zero temperature for the sake of simplicity, although the formalism applies equally at finite temperatures.

In Fig. 6, we show the dispersion of the intersubband SDW above the FM ground state. As mentioned earlier, these two intersubband SDW modes $\omega_\pm(q)$ correspond respectively to transitions $|0\uparrow\rangle \rightarrow |1\downarrow\rangle$ and $|1\uparrow\rangle \rightarrow |0\downarrow\rangle$. The frequencies $\omega_\pm$ increase as functions of q, approaching asymptotic values $\omega_\pm(q\rightarrow\infty) = \omega_\pm^0 + |v_x|$, where $\omega_\pm^0$ are the non-interacting excitation energies and v_x is the exchange energy of the electron in the ground state. Mode coupling, which pushes down $\omega_-(q)$ and hence helps mode softening, is most visible at $q \rightarrow 0$. At zero layer separation, mode-coupling disappears, and we recover previously known results.[11,12] In Fig. 7, we show the intersubband SDW dispersion above the SYM state. The results are qualitatively similar to those in Fig. 6, except that there is no mode coupling in the symmetric state because Coulomb interaction is spin independent. The important thing to be noticed is that the long wavelength collective excitations are gapped in both the symmetric phase and the spin polarized phase. However, the mode softening does occur at the phase boundaries, as we show below.

To illustrate the phase instability, we show, in Fig.8, the lower-energy branch of the intersubband SDWs at $q = 0$ as a function of interlayer tunneling. We see that $\omega_-(q=0)$ indeed softens when approaching the phase boundaries from both the symmetric phase and the spin polarized phase, and remains zero inside the canted antiferromagnetic phase. The canted antiferromagnetic order parameter, calculated in the previous section, is also shown in Fig.8 for comparison purpose. We notice that the phase boundaries determined from these two independent approaches agree completely, as shown in the figure. The softening of the collective mode and the appearance of the antiferromagnetic order parameter implies that we have discovered a quantum phase transition in double-layer QH systems.

In Fig.9, the collective intersubband SDW dispersions in the canted antiferromagnetic

QH state are shown. The first thing to be noticed is that the lower energy branch $\omega_-(q)$ is a gapless mode. The existence of such a gapless Goldstone mode is due directly to the canted antiferromagnetic spin ordering which spontaneously breaks the spin-rotational symmetry of the Hamiltonian. This Goldstone mode is found to be linear in the long wavelength limit, consistent with the fact that it describes antiferromagnetic fluctuations. The existence of the gapless excitation in the canted antiferromagnetic phase implies that some thermodynamic quantities, such as specific heat, have power-law temperature dependence in the canted antiferromagnetic phase in contrast to their exponential temperature dependence in the normal (symmetric or ferromagnetic) phases.

Simple expressions governing the phase boundaries can be derived from the mode softening. The boundary between the symmetric (SYM) phase and the canted antiferromagnetic (C) phase is found to satisfy the following equation

$$(\Delta_{\rm sas} - U_-)^2 = U_-^2 + \Delta_z^2, \tag{2.23}$$

where $U_- = \tilde{V}_-(q=0) = \frac{1}{\Omega}\sum_{\mathbf{p}} e^{-p^2 l_o^2/2} V_-(p)$. It should be noted that, for any given $\Delta_{\rm sas}$, the critical layer separation at this boundary is considerably smaller than the critical layer separation where the charge density excitation in the $\nu = 1$ state becomes soft.[12] The reason for this is the absence of Hartree contribution to the SDW excitations. The boundary between the spin polarized (FM) phase and the canted antiferromagnetic (C) phase is found to satisfy

$$(\Delta_z + U_-)^2 = U_-^2 + \Delta_{\rm sas}^2. \tag{2.24}$$

The simplicity of Eqns. (2.23) and (2.24) makes the phase diagram easy to construct. It is worthwhile to note that the phase boundaries are determined by only three energy scales Δ_z, $\Delta_{\rm sas}$, and U_- in spite of the fact that the Hamiltonian is determined by four independent energy scales Δ_z, $\Delta_{\rm sas}$, and $V_\pm(q)$, of which the inter- and intra-layer interactions $V_\pm(q)$ are in fact continuous functions of wavelength q. This unexpected dependence of the phase diagram (Fig. 10) on just three energy scales which are entirely determined by the magnetic field, the

sample parameters (i.e. inter-layer separation, well width, etc.), and the tunneling strength, is a specific result of the Hartree-Fock approximation. The zero temperature phase diagram can thus be expressed as a function of two independent dimensionless variables $\Delta_z/\Delta_{\rm sas}$ and $U_-/\Delta_{\rm sas}$, as shown in Fig. 10. This phase diagram applies to all double-layer quantum Hall systems at $\nu = 2$ which may have any values of Zeeman energy, tunneling energy, layer separation, layer-thickness, etc. We believe, however, that this remarkable scaling in the phase diagram (which enables us to reduce an infinite number of Δ_{sas} versus d diagrams for various values of Δ_z, of which examples are shown in Fig. 4, to just one phase diagram shown in Fig. 10) remains approximately valid, although the relative size of various phases in the universal phase diagram of Fig. 10 may very well be quantitatively not particularly accurate. We also mention here that this phase diagram is topologically identical to that of a $(2+1)$–dimensional quantum $O(3)$ nonlinear σ-model in a magnetic field,[9] as discussed in section III of this paper.

In this subsection, we have studied the collective intersubband SDW excitations for $\nu = 2$ double-layer QH systems in the time dependent Hartree-Fock approximation. We have presented the dispersions of the collective SDW excitations in both the normal QH phases (FM and SYM) and in the canted antiferromagnetic QH phase, and investigated the mode softening which signals the phase instabilities. We have rederived the same phase diagram as that obtained in the previous section, and obtained analytic equations for the two phase boundaries separating the new canted antiferromagnetic phase from the normal FM and SYM phases.

C. Kosterlitz-Thouless transition

In this subsection, we discuss some thermodynamic properties of $\nu = 2$ double-layer systems which arise from the spontaneous symmetry-breaking associated with the breaking of $U(1)$ planar spin rotational symmetry in the canted antiferromagnetic quantum Hall phase. There should be a finite temperature Kosterlitz-Thouless transition in the canted

antiferromagnetic phase, since the spin-rotational $U(1)$ symmetry is broken. Below the critical temperature, the system supports a linear Goldstone mode, which gives rise to a power-law temperature dependence for the specific heat. Above the critical temperature the $U(1)$ symmetry is restored and the system is paramagnetic. These properties are, in principle, experimentally observable and provide direct ways to test our theory.

We can estimate the Kosterlitz-Thouless transition temperature for our problem in the following manner. In the canted antiferromagnetic phase, the low temperature thermodynamics is governed by long wavelength phase fluctuations of the order parameter. Let $E_\phi = \langle\phi|H|\phi\rangle - \langle|H|\rangle$, where $|\rangle$ is the ground state of the canted antiferromagnetic phase, and $|\phi\rangle = \exp(i\sum_j S_j^z\phi_j)|\rangle$, with S_j^z as the spin operator of the j-th electron and $\hat{z}$ is the (magnetic field) direction normal to the two dimensional plane. In the long wavelength limit, one obtains

$$E_\phi = \frac{\rho_s(\Delta_z)}{2}\int d^2r|\bigtriangledown\phi(\mathbf{r})|^2, \tag{2.25}$$

with

$$\rho_s(\Delta_z) = \frac{l_o^2}{16\pi^2}\int_0^\infty q^3 e^{-l_o^2q^2/2}\left[v_a(q)\left(\frac{\sin\theta_1+\sin\theta_2}{2}\right)^2 + v_e(q)\left(\frac{\sin\theta_1-\sin\theta_2}{2}\right)^2\right]dq, \tag{2.26}$$

where l_o is the magnetic length and v_a (v_e) is intralayer (interlayer) Coulomb potential. For future convenience, we have written the stiffness as an explicit function of Δ_z, which arises from the dependence of the angles $\theta_{1,2}$ on the Zeeman splitting. The effective planar XY model defined by Eq. (2.25 undergoes a Kosterlitz-Thouless phase transition[18] at approximately $k_BT_c = (\pi/2)\rho_s(\Delta_z)$. Finite temperature spin-wave and vortex-antivortex polarizations reduce the transition temperature to approximately[3,4,19]

$$k_BT_c \approx 0.90\rho_s(\Delta_z). \tag{2.27}$$

These finite temperature renormalizations can be much larger in the vicinity of the C–N and C–SYM phase boundaries: the expression (2.27) can then no longer be used, and we will discuss modifications near these boundaries later in Section III.

Since we know $\rho_s(\Delta_z)$ exactly within the microscopic Hartree-Fock approximation, the Kosterlitz-Thouless transition temperature can be easily determined for our problem. In Fig. 11, we show the calculated Kosterlitz-Thouless critical temperature in $\nu = 2$ double-layer quantum Hall systems within the mean-field Hartree-Fock approximation (i.e. from Eq. (2.26) for $\rho_s(\Delta_z)$). The phase transition exists only in the canted antiferromagnetic quantum Hall phase. The critical temperature vanishes at the phase boundaries as the symmetry-breaking order parameter drops continuously to zero as the phase boundaries are approached from within the canted antiferromagnetic phase. We notice that the calculated Kosterlitz-Thouless temperature ($\sim 1K$) is well within the experimentally accessible regime for typical AlGaAs/GaAs–based double-layer systems. The effective spin-stiffness $\rho_s(\Delta_z)$ given in Eq. (2.26) is obtained in the mean-field Hartree-Fock approximation, i.e. using the results from sections II A and II B, where quantum fluctuation effects are not included. The results in Fig. 11 should thus be regarded as the upper bound for the Kosterlitz-Thouless critical temperature. We emphasize that the Kosterlitz-Thouless transition discussed here is present even in the presence of interlayer tunneling (in fact, the presence of finite interlayer tunneling is essential to stabilize the canted antiferromagnetic phase, as described in the last two sections), unlike the case associated with the pseudospin transition[3,4] at $\nu = 1/m$ (m odd integers) where interlayer tunneling suppresses Kosterlitz-Thouless transition.

Below the Kosterlitz-Thouless transition temperature, the specific heat in the antiferromagnetic phase has qualitatively different temperature dependence from those of the normal quantum Hall phases. This is of practical significance since it is possible to experimentally measure the specific heat of quantum Hall systems.[20] At low temperatures, the main contribution to the specific heat comes from long wavelength low energy intersubband SDWs. With their dispersions calculated in each of the quantum Hall phases, the heat capacity is easily obtained: $C = (\partial/\partial T)\sum_{\mathbf{k}}\langle n_-(k)\rangle\omega_-(k)$, where $\omega_-(k)$ is the energy of the low-lying intersubband SDW excitation and $\langle n_-(k)\rangle$ is its Bose occupation factor. The results are shown in Fig. 12. It is clear that the specific heat has an activated behavior in the normal quantum Hall phases because of the existence of excitation gap in its spin wave spectra,

and a quadratic power-law temperature dependence in the canted antiferromagnetic phase because of the existence of the linear Goldstone mode in the symmetry broken phase. The spin stiffness goes to zero discontinuously at T_c, and for $T > T_c$ we have the usual disordered X–Y phase of the Kosterlitz-Thouless transition.

D. Multicritical points

Our analysis so far has obtained solutions for the FM, SYM and C phases obtained by varying the parameters Δ_z, $\Delta_{\rm sas}$, d in the Hamiltonian (see Figs. 4 and 10) which modify the relative strengths of the Zeeman energy, the tunneling energy, and the Coulomb interaction energy, respectively. Generically, these phases separated by phase boundaries representing second-order quantum transitions. However, there are also special quantum multicritical points in Figs 4 and 10 whose physical significance we will now discuss.

The first quantum multicritical point is apparent in Fig. 4 where the FM, C and SYM phases come together at a single point on the abscissa corresponding to vanishing interlayer separation ($d = 0$). It is easily noted from Fig. 4 that this quantum multicritical point is in fact defined by

$$\Delta_{\rm sas} = \Delta_z; \qquad d = 0, \tag{2.28}$$

which is equivalent to the conditions

$$\Delta_{\rm sas} = \Delta_z; \qquad V_-(q) = 0, \tag{2.29}$$

using the definition of $V_\pm(q)$ given immediately following Eq. (2.3) in section II A. The simple physical reason for the vanishing of $V_-(q)$ along the $d = 0$ line is that the intra- and interlayer Coulomb interactions are identical in the limit of vanishing interlayer separation d. Note also that the vanishing of V_- (and consequently of U_-) pushes the quantum multicritical point to an infinite value of the abscissa ($\Delta_{\rm sas}/U_- \to \infty$) in the scaled universal diagram given in Fig. 10— in Fig. 10 the two phase boundaries separating the three phases

approach each other asymptotically as $\Delta_{\rm sas}/U_- \to \infty$ and $\Delta_z/\Delta_{\rm sas} \to 1$ at the multicritical point. Note that the condition $\Delta_z = \Delta_{\rm sas}$ for the quantum multicritical point is a particularly interesting criterion because, in the absence of our predicted canted antiferromagnetic phase (i.e. if the $\nu = 2$ double-layer QH systems allowed only the ferromagnetic and the symmetric phases, as was assumed in the literature before our work), the condition of the equality of the Zeeman splitting and the symmetric-antisymmetric gap (i.e. $\Delta_z = \Delta_{\rm sas}$) is precisely the single particle *level crossing* criterion where, at $\nu = 2$, one would make a transition from the ferromagnetic phases where the two up-spin symmetric and antisymmetric levels are occupied and the down-spin levels are empty for $\Delta_z > \Delta_{\rm sas}$ to the symmetric (spin singlet) phase where the spin-up and spin-down symmetric subbands are occupied (and the antisymmetric levels are empty) for $\Delta_{\rm sas} > \Delta_z$. What our theory definitely predicts is that such a simplistic one particle level crossing picture (which appears to be obvious intuitively) *does not occur* in a double-layer QH system at $\nu = 2$— instead Coulomb interaction breaks the $SU(2)$ spin rotational symmetry and drives the system into an intervening antiferromagnetic phase where spin and pseudospin levels are intrinsically mixed. The fact that the intuitively expected level crossing phenomenon (at $\Delta_z = \Delta_{\rm sas}$) has never been observed[38] in a $\nu = 2$ double-layer QH system in spite of systematic efforts[39] is, in our opinion, rather strong indirect evidence in support of our phase diagram.

The second multicritical point becomes apparent only in the universal phase diagram shown in Fig. 10 (and can be inferred implicitly from the trend that can be seen in the phase diagrams shown in Fig. 4). Its existence is a consequence of the intriguing finding that our antiferromagnetic state, in fact, persists all the way to $\Delta_z = 0$ (as can be clearly seen in Fig. 10 where a finite region of the antiferromagnetic state exists along the $\Delta_z = 0$ line) where the spin-polarized ferromagnetic phase no longer exists, and the antiferromagnetic phase is separated from the spin singlet phase by a multicritical point (M) defined by the condition

$$\Delta_{\rm sas} = 2U_- \quad \text{with} \quad \Delta_z = 0. \tag{2.30}$$

Thus the critical line defining the phase boundary between the antiferromagnetic and the symmetric phases for $\Delta_z \neq 0$ ends at a critical point (M) for $\Delta_z = 0$. It is evident that in the absence of any Zeeman energy ($\Delta_z = 0$) the spin magnetic moment in each layer lies completely in the 2D plane of the electron gas where they must be equal and opposite in the two layers. Therefore, the $\Delta_z = 0$ antiferromagnetic phase of Fig. 10 is *not* a *canted* phase, but is a purely Néel phase (N); indeed the Hamiltonian has full $SU(2)$ spin rotation symmetry for $\Delta_z = 0$, and spin moments in the N phase can point in any two anti-parallel directions. The N, C, and SYM phases meet at the multicritical point M. This multicritical point will take on special significance in our effective field theoretical formulation in the next section.

Let us also note that the existence of this purely Néel QH antiferromagnet at $\nu = 2$ double-layer system may not be just a theoretical curiosity because it is possible to obtain vanishing Zeeman splitting in a GaAs double-layer system in a finite magnetic field situation by applying external pressure which under suitable conditions could lead to the vanishing of the effective gyromagnetic ratio (the g-factor) due to band structure effects.

E. Comparison with earlier work

Before concluding this section, and going on to the effective field theoretic description of the double-layer QH system, we will discuss the relationship of our results to some earlier work on double layer systems. We will also use this opportunity to comment on the validity of the Hartree Fock approximation in our and earlier work.

Most earlier studies,[2–4,12] however, have focused on $\nu = 1$ (with some work[5] on $\nu = 1/2$). Although the $\nu = 1$ and the $\nu = 2$ QH systems exhibit some similarities such as the softening of their low energy collective excitations under certain conditions, there are important distinctions between them. At $\nu = 1$, the spin degree of freedom is normally frozen out by the external magnetic field. The relevant low energy excitations in the $\nu = 1$ QH state are therefore intersubband charge-density-wave excitations, and the properties of the

system are determined by the interplay between interlayer tunneling energy and Coulomb interaction energy. In this sense, the $\nu = 1$ system is in fact a single-layer system with a layer pseudospin-dependent interaction.[3,4,12] At $\nu = 2$, both the spin degree of freedom and the layer degree of freedom are relevant, and the low energy excitations are intersubband SDW excitations. Consequently, the properties of the system are determined by the interplay among tunneling energy, Zeeman energy, and Coulomb interaction energy. Because of the increased degree of freedom, the system has more ways to optimize the total energy, and new states which are not possible at $\nu = 1$ become possible at $\nu = 2$. The symmetric QH state is energetically favored at small layer separations because it optimizes the tunneling energy; The spin polarized QH state is favored at large layer separations because it optimizes the Coulomb interaction energy; The canted antiferromagnetic state is energetically favored at intermediate layer separations. The reason for this is that the canted antiferromagnetic state tends to simultaneously optimize both the tunneling energy and the Coulomb interaction energy, which prevails at intermediate layer separations where the tunneling energy and the Coulomb interaction energy are equally important. Both the canted antiferromagnetic state and the symmetric state exist only for systems with small enough Zeeman energy, as the Zeeman energy clearly favors the spin polarized state.

Another important distinction between the $\nu = 1$ systems and the $\nu = 2$ systems is that although at $\nu = 1$ the mode softening destroys the QH effect[12], and there is no reliable description of the electronic state in the non-QH phase because beyond the critical layer separation the system becomes effectively a pair of isolated layers with compressible half-filled Landau level states; in contrast, at $\nu = 2$, the QH effect prevails at all phases because there is always a charge gap in both layers (even as $d \to \infty$), and we have good understanding of the ground state and the low energy excitations in each phase due to the existence of incompressible filled Landau levels. Nevertheless, the mode softening and the associated phase transitions at $\nu = 2$ are likely to be observable through inelastic light scattering experiments[8,13] and thermodynamic measurements.

Our work has studied $\nu = 2$ double-layer systems by numerically solving the self-

consistent mean-field equations[10], and obtained collective excitation dispersions using many-body diagrammatic techniques.[11] Both approaches are, however, based on the Hartree-Fock approximation. In single-layer integer QH systems, calculations[11] in the Hartree-Fock approximation agree well with experiments.[13] In double-layer systems, the Hartree-Fock approximation is less accurate because Coulomb interaction potential is layer-index dependent. Nevertheless, we expect that the Hartree-Fock approximation remains a reasonably good description for a double-layer system at $\nu = 2$, since the Hartree-Fock ground state, which is non-degenerate and separated in energy from higher levels, is a good approximation for the real many-body ground state at $\nu = 2$ due to the existence of incompressible filled Landau level states with charge excitation gaps at any layer separations. We want to especially emphasize the difference in the validity of the Hartree-Fock approximation between $\nu = 1$ and $\nu = 2$. The approximation is valid at $\nu = 1$ only at small layer separations and fails completely beyond a critical layer separation where the system becomes effectively a pair of isolated layers with compressible half-filled Landau level state in each layer. At $\nu = 2$, incompressible states with filled Landau levels exist at any layer separations. In particular, there is still one filled Landau level in each layer at $d \to \infty$. This fact, namely the existence of an incompressible energy gap at all layer separations, ensures that the Hartree-Fock approximation, upon which our calculations are based, is a reasonable formalism at $\nu = 2$ regardless of the value of the layer separation.

III. CONTINUUM FIELD THEORY AND QUANTUM CRITICAL PHENOMENA

The Hartree-Fock analysis used in the previous sections has the advantage of working with a realistic microscopic Hamiltonian and of making definite quantitative predictions for experimental observables in realistic samples. In this section, we will present an alternative analysis based upon a continuum effective quantum field theory for the low-lying spin excitations of a double layer quantum Hall system. We will find that the global phase diagrams obtained in the two approaches are very similar, and are, in fact, topologically identical, and

that detailed additional predictions for the temperature dependence of various observables can be made by a combination of the two methods. In particular, some advantages offered by the continuum approach are:

- It will become clear from the analysis below that there are two basic ingredients necessary to obtain the phases of Fig 10: two well separated layers form fully polarized ferromagnets with a gap towards charged excitations (i.e. an incompressible QH effect gap), and the primary coupling between the layers is an antiferromagnetic exchange (i.e. a superexchange) interaction. As such, we expect a similar phase diagram to apply not only at filling $\nu = 2$, but also at any $\nu = 2\nu_1$, where ν_1 is any filling fraction where a single layer has a charge gap, and is fully polarized. In particular, this criterion is satisfied at $\nu = 2/m$, m an odd integer, where each layer forms a polarized Laughlin fractional quantum Hall state. The Hartree-Fock analysis clearly cannot be applied for $m > 1$, as the single layer charge gap appears only after inclusion of the non-trivial correlations implicit in the Laughlin state.

- The Hartree-Fock theory significantly overestimates the energy of the spin-unpolarized symmetric (SYM) or the spin singlet (SS) state, as we will refer to it in this section. Spin up and spin down electrons are simply placed into the same orbitals which are symmetric in the layer index. This is costly in Coulomb energy as there are no correlations in the layer positions of the up and down spin electrons. It is clearly more advantageous to form a spin singlet states between electrons which are localized in opposite layers. The non-linear sigma model continuum field theory to be discussed below does this in a natural way. From now on in this section we refer to this symmetric or the spin singlet phase as the SS to emphasize its correlated singlet nature.

- A number of quantum-critical points have been uncovered in the Hartree-Fock analysis. There is the $\Delta_z = 0$ quantum critical point between the spin singlet (SS or SYM) and the Néel (N) phases, and a critical line between the SS and the canted antiferromagnetic (C) phases. Our continuum approach will obtain the critical theory for these

transitions, and we will find that they have dynamic critical exponents[40] $z = 1$ and $z = 2$ respectively. There is also a second critical line between the C and the fully spin polarized ferromagnetic (FM) phases: this transition has $z = 2$ and will be discussed only in passing, as the critical theory is rather similar to one of the models discussed in detail in Ref 27.

- The continuum theory offers not only provides us the zero temperature quantum phase diagram but also a streamlined approach to the study of properties at non-zero temperature, especially in the vicinity of the quantum critical points where effects of fluctuations cannot be neglected. The price one pays is that in general the parameters defining the effective field theory are quantitatively unknown and can only be calculated from a microscopic theory such as the Hartree-Fock theory of the previous sections.

We motivate our formulation of the continuum theory by consideration of the physics of two well-separated identical layers at $\nu = 2/m$. More specifically, the layer separation, d, is much larger than the magnetic length, ℓ_o. Then the two layers (labeled 1,2) are approximately decoupled, and each separately has filling fraction $\nu_1 = \nu_2 = 1/m$. Their ground states will be the familiar Laughlin states for $m > 1$, or a fully filled lowest Landau level at $m = 1$, both of which are incompressible states with large energy gap to all charged excitations. These states are also fully spin polarized; the spin polarization is induced not just by the Zeeman coupling to the external magnetic field, but also by the significantly larger intralayer ferromagnetic exchange[3,4,22]. The low-lying excitations in each layer are spin waves which have a small excitation gap given precisely by the Zeeman energy $\Delta_z = g\mu_B B$. For small g, a complete description[4,24] of the low energy excitations of each layer can be given in terms of an action for unit vector fields $\vec{n}_{1,2}$ ($\vec{n}_{1,2}^2 = 1$) representing the orientation of the ferromagnetic orders. Spin waves are small fluctuations of $\vec{n}_{1,2}$ about an ordered state, while charged quasiparticles are Skyrmion[4,21–23] textures of $\vec{n}_{1,2}$. The effective action describing the two layers is[3,4,22,24] (in units with $\hbar = k_B = 1$)

$$\mathcal{S}_0 = \int d^2x \int_0^{1/T} d\tau \left(\mathcal{L}_F[\vec{n}_1] + \mathcal{L}_F[\vec{n}_2]\right)$$
$$\mathcal{L}_F[\vec{n}] \equiv iM_0\vec{A}(\vec{n}) \cdot \frac{\partial \vec{n}}{\partial \tau} + \frac{\rho_s^0}{2}\left(\nabla_x \vec{n}\right)^2 - M_0\Delta_z n_z \tag{3.1}$$

Here

$$M_0 = \frac{1}{4\pi m \ell_o^2} \tag{3.2}$$

is the magnetization density per layer, with l_o the magnetic length. The spin stiffness of each well separated layer is represented by ρ_s^0; for $m = 1$, we have the exact result[11] $\rho_s^0 = e^2/(16\sqrt{2\pi}\epsilon\ell_o)$, while for $m > 1$ numerical estimates of ρ_s^0 are given in Ref[22]. The term involving $\vec{A}$ accounts for the Berry phase accumulated under time evolution of the spins; here $\vec{A}$ is any functional of $\vec{n}$ which satisfies

$$\epsilon_{ijk}\frac{\partial A_k(n)}{\partial n_j} = n_i. \tag{3.3}$$

This Berry phase term also has a "dual" interpretation in the picture in which $\mathcal{L}_F$ is viewed as an action for Skyrmions[24,35]: it represents the coupling of the Skyrmion current to a "magnetic field" of strength $4\pi M_0$.

Now imagine reducing the value of d to couple the two layers. As there is a charge gap in each layer, we can neglect all charge transfer processes, and focus solely on spin exchange. Because of the strong repulsive interactions within each layer, we expect by an extension of the familiar arguments made in the context of the Hubbard model that there will be an *antiferromagnetic* superexchange coupling between the layers. This can also be inferred easily by considering the leading effect of interlayer tunneling and Pauli principle, which immediately provides a superexchange coupling between the layers. The complete double layer action is therefore

$$\mathcal{S}_1 = \int d^2x \int_0^{1/T} d\tau \left(\mathcal{L}_F[\vec{n}_1] + \mathcal{L}_F[\vec{n}_2] + J\vec{n}_1 \cdot \vec{n}_2\right) \tag{3.4}$$

The value of the interlayer exchange, J, is not known precisely; we expect that it is of order $J \sim M_0\Delta_{\rm sas}^2/U$ where $\Delta_{\rm sas}$ is the tunneling matrix element (see Eq. (2.2), for example)

between the layers, and $U \sim e^2/\epsilon\ell_o$ is the Coulomb repulsion energy. In addition to the imprecisely known J, the present approach also requires knowledge of the nature of the short distance cutoff at lengths of order ℓ_0 beyond which present continuum approach cannot be applied. We will show later that our ignorance of these quantities can be reduced entirely to uncertainties in the value of a certain renormalized energy scale. This energy scale can be either measured directly in an experiment, or computed by any microscopic theory such as the Hartree-Fock approach (appropriate at $\nu = 2$) described in sections II A–II C. Apart, from this single energy scale, however, all of the predictions of the present effective field theoretical approach will be quantitative and precise.

Some potentially important terms have been omitted from $\mathcal{S}_0$ and our analytic computations: the Hopf term which endows the Skyrmions with fractional statistics, and the long-range Coulomb interaction between the Skyrmions. We believe this is permissible because of the charge gap. Further[25], as the layers are antiferromagnetically correlated, Skyrmions in one layer will be correlated with anti-Skyrmions in the other, and this neutralizes the leading contribution of both terms. This latter argument should continue to hold even if the charge gap were to vanish at a quantum critical point (the charge gap remains non-zero at the quantum critical points in both our present calculations). Note also that no new term is necessary to induce charge transfer between the layers: a hedgehog/anti-hedgehog pair in the two layers corresponds to an event transferring Skyrmion number between them. Such spacetime singularities are absent in the strict continuum limit but appear when a short-distance regularization is introduced.

For completeness, we note that the purely $\vec{n}$ field formulation becomes incomplete for $m > 1$ and larger g, as the spin zero Laughlin quasiparticles can become the lowest energy charged excitations. These should, in principle, be accounted for by a separate complex scalar field. However, these can also be neglected for the same reasons presented above for non-zero spin charged excitations.

We now manipulate the effective action into a form more suitable for our subsequent analysis. We solve the constraints $\vec{n}_{1,2}^2 = 1$ by representing

$$\vec{n}_i = (-1)^i (1 - \vec{L}^2)^{1/2} \vec{n} + \vec{L} \tag{3.5}$$

where $\vec{n}$ and $\vec{L}$ are vectors satisfying

$$\vec{n}^2 = 1 \qquad \vec{L} \cdot \vec{n} = 0. \tag{3.6}$$

Note that this representation is so far exact. Next, we insert (3.5) into $\mathcal{S}_1$. Because the layers are antiferromagnetically correlated we expect that $\vec{L}$ will not be too large, and it is therefore permissible to expand the resulting action to quadratic order in $\vec{L}$. This is clearly an approximation: in Appendix A we examine a model solvable Hamiltonian by the same method in order to assess the damage done by neglecting terms higher order in $\vec{L}$—we find that this procedure obtains the low energy spectrum correctly but introduces some spurious states at higher energies. To quadratic order in $\vec{L}$, $\mathcal{S}_1$ takes the form

$$\mathcal{S}_1 = \int d^2x \int_0^{1/T} d\tau \left[2iM_0 \vec{L} \cdot \left(\vec{n} \times \frac{\partial \vec{n}}{\partial \tau} + i\Delta_z \hat{z} \right) + \rho_s^0 \left(\nabla_x \vec{n} \right)^2 + 2J\vec{L}^2 \right], \tag{3.7}$$

where $\hat{z}$ is a unit vector in the direction of the magnetic field. Now we integrate out $\vec{L}$ while maintaining the constraint $\vec{L} \cdot \vec{n} = 0$ by adding an additional term to the energy $\sim C(\vec{L} \cdot \vec{n})^2$ and then taking the limit $C \to \infty$. This yields the following effective action for the antiferromagnetic order parameter $\vec{n}$

$$\mathcal{S}_2 = \frac{c}{2t} \int d^2x \int_0^{1/T} d\tau \left[\left(\nabla_x \vec{n} \right)^2 + \frac{1}{c^2} \left(\frac{\partial \vec{n}}{\partial \tau} - i\Delta_z \hat{z} \times \vec{n} \right)^2 \right] \tag{3.8}$$

where

$$t = \left(\frac{J}{2\rho_s^0 M_0^2} \right)^{1/2} \qquad c = \left(\frac{2\rho_s^0 J}{M_0^2} \right)^{1/2}. \tag{3.9}$$

This is precisely the action of the 2+1 dimensional quantum $O(3)$ non-linear sigma model in a field B coupling to the conserved global $O(3)$ charge.[26–29] It is expected to apply to double-layer quantum Hall systems with $\nu = 2/m$ at length scales larger than $\Lambda^{-1} \sim \ell_o$.

The remainder of this section consists of a detailed analysis of the properties of $\mathcal{S}_2$. The techniques and some results have already been presented earlier in Refs 26,27,29: we shall present here a unified treatment with a special emphasis on dynamical properties at non-zero temperature. We begin in Section III A by developing a simple mean-field phase diagram of $\mathcal{S}_2$.

A. Mean field theory

This section will summarize the results of the application of the mean field theory of Ref 27 to the action $\mathcal{S}_2$. Formulation of the mean field theory requires some short distance regularization, and we choose to place the continuum theory on a square lattice in the spatial directions, with a lattice spacing $a \sim \ell_o$; a continuum formulation is maintained along the time direction. The resulting action is equivalent to the following lattice quantum rotor Hamiltonian

$$\mathcal{H} = \sum_i \left(\frac{f}{2} \hat{\vec{L}}_i^2 - \Delta_z \hat{z} \cdot \hat{\vec{L}}_i \right) - K \sum_{<i,j>} \hat{\vec{n}}_i \cdot \hat{\vec{n}}_j \tag{3.10}$$

where the coupling constants in $\mathcal{H}$ are

$$f = \frac{ct}{a^2} \qquad\qquad K = \frac{c}{t} \tag{3.11}$$

The Hamiltonian is expressed in terms of operators $\hat{\vec{n}}_i$ which represent the orientation of the rotors, and $\hat{\vec{L}}_i$ which are the rotor angular momenta. The operators on different sites commute, while those on a single site obey the commutation relations (dropping the site indices)

$$\begin{aligned} \left[\hat{L}_\alpha, \hat{L}_\beta\right] &= i\epsilon_{\alpha\beta\gamma}\hat{L}_\gamma \\ \left[\hat{L}_\alpha, \hat{n}_\beta\right] &= i\epsilon_{\alpha\beta\gamma}\hat{n}_\gamma \\ \left[\hat{n}_\alpha, \hat{n}_\beta\right] &= 0 \end{aligned} \tag{3.12}$$

We will describe the properties of $\mathcal{H}$ by choosing the best among the mean field Hamiltonians given by[27]

$$\mathcal{H}_{MF} = \sum_i \left(\frac{f}{2} \hat{\vec{L}}_i^2 - \Delta_z \hat{z} \cdot \hat{\vec{L}}_i - KZ\vec{N} \cdot \hat{\vec{n}}_i \right) \tag{3.13}$$

Here Z $(= 4)$ is the lattice co-ordination number, and $\vec{N}$ is a variational parameter to be chosen so that the expectation value of $\mathcal{H}$ in the ground state of $\mathcal{H}_{MF}$ is as low as possible; by the usual argument, this is expected to happen when $\vec{N} = \langle \hat{\vec{n}} \rangle$.

As in Ref 27, we numerically diagonalized $\mathcal{H}_{MF}$ by truncating its spectrum at some large angular momentum, and then optimized the value of $\vec{N}$. The resulting phase diagram is shown in Fig 13. We discuss the properties of the various phases in turn:

1. Spin Singlet (SS or SYM)

Each rotor is in its non-degenerate $\ell = 0$ state, $\vec{N} = 0$, and there is a gap to all excitations. The ground state is a spin singlet, and is therefore unaffected by variations in the value of Δ_z.

2. Quantized Ferromagnets (QF_ℓ)

Again, $\vec{N} = 0$, each rotor now has azimuthal angular momentum $m = \ell$ and this value remains pinned as various parameters are varied. Each rotor is also in precisely the state with $\hat{\vec{L}}^2 = \ell(\ell + 1)$, although this latter feature is a special property of mean field theory which will not survive fluctuations. Of these phases, only the $\ell = 1$ case is actually allowed for the double layer action $\mathcal{S}_1$, and it is clearly the FM phase of Fig 10. The other phases are an artifact of the approximations made in mapping $\mathcal{S}_1$ to $\mathcal{S}_2$: this should be clear from the discussion in Appendix A where we show that expanding in powers of $\vec{L}$ introduce spurious higher angular momenta states.

3. Canted (C) and Néel (N) States

These states have $\vec{N} \neq 0$ and varying continuously as the parameters are varied; we have $N_x \neq 0$, $N_y \neq 0$ and $N_z = 0$. From (3.5), this implies that the two layers have opposite spin

polarizations in the $x-y$ plane. The two layers also have an identical ferromagnetic polarization, given by $\langle \hat{\vec{L}} \rangle$ which is oriented along the z direction. This ferromagnetic moment varies continuously as parameters are varied, and vanishes when $\Delta_z \to 0$. So for general $\Delta_z \neq 0$ this state is canted (C), while for $\Delta_z = 0$ it is a pure Néel (N) antiferromagnet. The C phase has a single linearly dispersing spin wave mode in the $x-y$ plane, while the N phase has two spin waves[27].

In the remainder of this section, we will present a detailed theory of the universal properties of the system in the vicinity of the multicritical point M. This is the same quantum multicritical point (M) which exists in the universal Hartree-Fock phase diagram of Fig. 10 where the N phase (along the $\Delta_z = 0$ line), the C phase and the SYM (SS) phase come together at $\Delta_{\rm sas} = 2U_-$. We point out in this context that the other distinct multicritical point of the Hartree-Fock theory where the canted antiferromagnetic phase, the ferromagnetic phase, and the symmetric phase coexist (the point on the abscissa defined by $d = 0$ and $\Delta_z = \Delta_{\rm sas}$ in Fig. 4) is not accessible within the effective field theory due to the long wavelength restriction $d > l_o$. (We mention that in our notations Δ_z in the Hartree-Fock theory corresponds to just B in the field theory due to our choice of units.)

Note that the C, N, and SS phases meet at M, and so we will also discuss the universal second-order transitions between them. We will not discuss the nature of the second-order transitions between the QF_ℓ and C phases: very closely related transitions, in the same universality class, have been discussed in some detail in Ref 27.

B. Zero temperature critical properties

A first study of the properties in the vicinity of the point M has appeared in Ref 26 using a large N expansion in a non-linear sigma model with N component fields. The issues of interest here are more conveniently obtained using a recently developed expansion[29] in spatial dimensionality, d, in powers of $\epsilon = 3 - d$. The latter approach is expressed in terms of a soft-spin field theory, and we therefore begin with a soft-spin version of the non-linear

sigma model $\mathcal{S}_2$:

$$\mathcal{S}_\phi = \int d^d x \int_0^{1/T} \left[\frac{1}{2} \left\{ (\partial_\tau \phi_x - i\Delta_z \phi_y)^2 + (\partial_\tau \phi_y + i\Delta_z \phi_x)^2 + (\partial_\tau \phi_z)^2 + c^2 (\nabla_x \vec{\phi})^2 + r\vec{\phi}^2 \right\} + \frac{u_0}{4!} (\vec{\phi}^2)^2 \right] \tag{3.14}$$

Here $\vec{\phi} \equiv (\phi_x, \phi_y, \phi_z) \sim \vec{n}$ is the soft-spin field which measures the staggered moment of the two layers. We have taken the magnetic field to point in the z direction. We will also be interested in the uniform ferromagnetic moment density of the system, M, and this is given by

$$M \equiv M_0 \langle n_{1z} + n_{2z} \rangle = -\frac{\partial \mathcal{F}}{\partial \Delta_z} \tag{3.15}$$

where $\mathcal{F}$ is the free energy density associated with the action $\mathcal{S}_\phi$. We have introduced two new coupling constants, r and u_0 in $\mathcal{S}_\phi$; these are related to the coupling t of $\mathcal{S}_2$, and its short-cutoff $\sim \ell_o$. We will not specify the precise values of these parameters here, as they merely appear at intermediate stages of our computation, and not in our final results.

Let us first discuss the mean field properties of $\mathcal{S}_\phi$, obtained simply by minimizing the action while ignoring all spatial and time dependence of $\vec{\phi}$. For $r - \Delta_z^2 > 0$, the ground state has $\langle \vec{\phi} \rangle = 0$, and is therefore in the quantum paramagnetic SS phase. For $r - \Delta_z^2 < 0$, the ground state has $\langle \vec{\phi} \rangle \neq 0$ and in the $x - y$ plane. This is the C phase and the fields have the expectation values

$$\vec{\phi} = \left(\left(\frac{6(\Delta_z^2 - r)}{u_0} \right)^{1/2}, 0, 0 \right) \qquad M = \frac{6\Delta_z (\Delta_z^2 - r)}{u_0}, \tag{3.16}$$

or any rotation of $\vec{\phi}$ in the $x - y$ plane. Notice that M vanishes for $\Delta_z = 0$, and therefore the line $r < 0$, $\Delta_z = 0$ is the N phase. The resulting mean field phase diagram is shown in Fig 14. Notice that the vicinities of the points M are very similar in Figs 13 and 14. The quantum critical point M is at $\Delta_z = 0$, $r = 0$, and it is clear from the Lorentz-invariant structure of $\mathcal{S}_\phi$ at $\Delta_z = 0$ that this point has dynamic exponent $z = 1$. Rotations of the order parameter $\vec{\phi}$ in the $x - y$ plane have associated with them a stiffness $\rho_s(\Delta_z)$ given by

$$\rho_s(\Delta_z) = \frac{6(\Delta_z^2 - r)}{u_0}. \tag{3.17}$$

This is the same stiffness which was computed in Section II C and Eqn 2.26 in the Hartree-Fock theory.

We now include the effects of fluctuations at one loop. We will quote results for the dynamic longitudinal and transverse susceptibilities of the $\vec{\phi}$ field which are measured in light scattering. Recall that in terms of the spin polarizations of the two layers $\vec{n}_1$, $\vec{n}_2$, we have $\vec{\phi} \sim \vec{n}_1 - \vec{n}_2$. We define (with T as the temperature $k_B = 1$ in our units in this section)

$$\chi_{\parallel}(i\omega) = \int d^d x \int_0^{1/T} d\tau e^{-i\omega\tau} \langle \phi_z(x,\tau)\phi_z(0,0)\rangle \tag{3.18}$$

and

$$\chi_{\perp}(i\omega) = \frac{1}{2}\int d^d x \int_0^{1/T} d\tau e^{-i\omega\tau} \langle (\phi_x(x,\tau) + i\phi_y(x,\tau))(\phi_x(0,0) - i\phi_y(0,0))\rangle \tag{3.19}$$

We can use the methods of Ref 29 to compute the one loop values of these susceptibilities in the SS phase (this is the phase with no broken symmetry) in the vicinity of the point M; we obtain

$$\begin{aligned} \chi_{\parallel}(\omega) &= \frac{1}{\Delta^2 - \omega^2} \\ \chi_{\perp}(\omega) &= \frac{1}{\Delta^2 - (\omega - \Delta_z)^2} \end{aligned} \tag{3.20}$$

Here the quantity Δ is an observable defined by

$$\Delta \equiv \text{Spin gap of the SS phase at } T = 0 \text{ for } r > 0 \text{ and } \Delta_z = 0. \tag{3.21}$$

The value of Δ should either be measured experimentally, or computed by a detailed microscopic calculation like the Hartree-Fock theory discussed earlier in the paper. We will express all our results for $r > 0$ completely in terms of universal functions of parameters Δ, T and B (so that the microscopic couplings r and u_0 do not appear anywhere in our results.) Clearly, in the mean field theory $\Delta = \sqrt{r}$; at one loop order, we have $\Delta \sim r^{\nu}$, where the exponent $\nu = 1/2 + 5\epsilon/44$.

We need a separate experimental observable to measure the deviation of the system from the point M at $\Delta_z = 0$ for $r < 0$. A convenient choice, also used in Refs 28,29 is the spin stiffness. We therefore define

$$\rho_s(0) \equiv \text{Renormalized spin stiffness of the N phase at } T = 0 \text{ for } r < 0 \text{ and } \Delta_z = 0. \quad (3.22)$$

All our results for $r < 0$ will be expressed in terms of $\rho_s(0)$. Again $\rho_s(0) \sim |r|^\nu$, and the actual value of $\rho_s(0)$ should be measured experimentally or computed in Hartree-Fock or microscopic numerical studies of the double-layer Hamiltonian.

Before closing this subsection, we draw attention to the fact that there are two phase boundaries that terminate at the point M: the SS to C transition and the N to C transition. In the vicinity of these transitions the response functions computed near the critical point M should turn into *reduced* scaling functions[29,36] characteristic of the respective phase transitions. In the following subsections, we discuss simplified versions of the action $\mathcal{S}_\phi$ which can be used to compute these reduced scaling functions.

1. SS-C transition, $|\Delta - \Delta_z| \ll \Delta$, $r > 0$

In this region we can neglect ϕ_z fluctuations and focus only on the $\phi_x + i\phi_y$ which is undergoing Bose condensation. Further, it can also be shown that the second-order time derivative in $\mathcal{S}_\phi$ can be dropped. Making these approximations, and defining

$$\Psi = \frac{\phi_x + i\phi_y}{\sqrt{\Delta_z}}, \quad (3.23)$$

we see that $\mathcal{S}_\phi$ reduces to

$$\mathcal{S}_\Psi = \int d^2x \int_0^{1/T} d\tau \left[\Psi^* \frac{\partial \Psi}{\partial \tau} + \frac{c^2}{2\Delta_z} |\nabla_x \Psi|^2 + (\Delta - \Delta_z)|\Psi|^2 + \frac{u_0}{24\Delta_z^2} |\Psi|^4 \right]. \quad (3.24)$$

This action has been previously studied in some detail[30,34]: it has a $z = 2$ quantum critical point at $\Delta = \Delta_z$, and we will use the existing results later. Thus the SS-C transition is a line of $z = 2$ critical points terminating in $z = 1$ critical end-point M.

2. N-C transition, $B \ll \rho_s(0)$, $r < 0$

Both the N and C phases are ordered, and it is sufficient to simply focus on static, thermal, orientational fluctuations of the order parameter. We therefore quench the magnitude

fluctuations of $\vec{\phi}$ and return to the fixed length vector $\vec{n}$. The effective action for static $\vec{n}$ fluctuations can be deduced from $\mathcal{S}_\phi$ to be

$$\mathcal{S}_n = \frac{1}{2T} \int d^2x \left[\rho_s(0) (\nabla_x \vec{n})^2 + \gamma n_z^2 \right]. \tag{3.25}$$

As noted earlier, $\rho_s(0)$ is the spin stiffness of the Néel state, fully renormalized by quantum fluctuations. The anisotropy $\gamma = 6\Delta_z^2(\Delta_z^2 - r)/u_0$ to lowest order in u_0, and we expect $\gamma \sim \Delta_z^2$ more generally. The action $\mathcal{S}_n$ has been studied in Ref 32, and we will use their results in the following subsection.

C. Non-zero temperature response functions

A number of new phenomena occur at non-zero temperatures, and these are addressed in a relatively straightforward manner using the present continuum effective field theory approach.

- There is a broken $x-y$ symmetry in the C phase, and therefore a non-zero temperature (T_c) at which this order disappears in a Kosterlitz-Thouless transition. An estimates T_c was given earlier (sections II C and Fig. 11) in the Hartree-Fock theory which is valid when the system is well away from one of the $T = 0$ phase boundaries of the C phase in Figs 13, and 14. We expect T_c to vanish continuously as the system in the C phase approaches the $T = 0$ boundaries to the N or the SS phase: there is nonzero temperature phase transition above the N or the SS ground state. We discuss below the behavior of T_c near the C-N and C-SS $T = 0$ phase boundaries. Near the point M, T_c is determined completely and universally by the two energy scales which measure the deviation of the ground state from M. So for $r > 0$ we expect

$$T_c = \Delta_z \Psi_> \left(\frac{\Delta}{\Delta_z} \right) \tag{3.26}$$

  where $\Psi_>$ is a fully universal function; because the SS-C phase boundary occurs precisely at $\Delta = \Delta_z$, we have

$$\Psi_>(u \geq 1) = 0. \tag{3.27}$$

Similarly for $r < 0$ we have

$$T_c = \Delta_z \Psi_< \left(\frac{\rho_s(0)}{\Delta_z} \right) \tag{3.28}$$

where $\Psi_<$ is also a universal function. Clearly the two functions should agree at $r = 0$, and therefore we have $\Psi_>(0) = \Psi_<(0)$; actually it is possible to say much more—for $\Delta_z > 0$ we expect that T_c is a smooth and analytic as a function of r through $r = 0$, and so using the dependencies of Δ and $\rho_s(0)$ on r, it is possible to express $\Psi_{>,<}$ as analytic continuations of each other. We will give explicit expressions for $\Psi_{>,<}$ to leading order in the expansion in $\epsilon = 3 - d$ below.

- The one-loop $T = 0$ results for the SS phase (3.20) predict infinitely sharp absorption peaks in $\chi_\parallel$ at $\omega = \Delta$, and in $\chi_\perp$ at $\omega = \Delta \pm \Delta_z$. As the SS phase has a spin gap, we expect these infinitely sharp peaks to survive at higher orders in the perturbation theory at $T = 0$. For $T > 0$ two qualitatively new features will arise. First, thermal damping will lead to a broadening of the peaks. Second, the peak positions will themselves become temperature dependent. We will describe these processes below in the vicinity of the point M, where both the broadening and the T-dependent shifts are quite significant. Deep inside the SS phase, well away from the M point, these T-dependencies are exponentially activated, and therefore much weaker.

We will restrict our results for the most part to the paramagnetic phase, although results in the magnetically ordered phases can be obtained by very similar methods. This means that we are working at $T > 0$ above the SS phase, and at $T > T_c$ above the C phase, all within the vicinity of the point M. The results are obtained using methods discussed in some detail in Ref 29: the only change is that the Zeeman splitting Δ_z has to be included in the propagators for the $\phi_{x,y}$ fields, and this modifies the values of the Matsubara frequency summations in the loop diagrams by replacing an energy ε by $\varepsilon \pm \Delta_z$. The reader may also

consult Appendix D of Ref 33 where a simpler derivation of just the one loop results of Ref 29 is given.

The non-zero T generalization of (3.20) takes the form

$$\chi_{\parallel}(\omega) = \frac{1}{-\omega^2 + m_{\parallel}^2 - i\Gamma_{\parallel}(\omega)}$$
$$\chi_{\perp}(\omega) = \frac{2}{-(\omega - \Delta_z)^2 + m_{\perp}^2 - i\Gamma_{\perp}(\omega)}$$

Here $m_{\parallel,\perp}$ and $\Gamma_{\parallel,\perp}$ depend implicitly upon the energy scales T, Δ_z, and Δ ($\rho_s(0)$) for $r > 0$ ($r < 0$) in a manner we shall describe below to lowest order in ϵ. Clearly, the "masses" $m_{\parallel,\perp}$ represent the peak absorption frequency, while $\Gamma_{\parallel,\perp}$ are the absorptive pieces which lead to a T-dependent broadening of the line.

First we describe the behavior of $m_{\perp,\parallel}$.

For $r > 0$, the masses are universal functions Δ, T and Δ_z. They can be written as

$$m_{\parallel}^2 = R_{\parallel} - \epsilon \frac{2\pi T}{11}\left(3\sqrt{R_{\parallel}} + 2\sqrt{R_{\perp}}\right)$$
$$m_{\perp}^2 = R_{\perp} - \epsilon \frac{2\pi T}{11}\left(\sqrt{R_{\parallel}} + 4\sqrt{R_{\perp}}\right) \tag{3.29}$$

where

$$R_{\parallel} = \Delta^2\left[1 + \frac{5\epsilon}{11}\ln\frac{T}{\Delta}\right] + \frac{\epsilon T^2}{11}\left[3G\left(\frac{\Delta^2}{T^2}, 0\right) + 2G\left(\frac{\Delta^2}{T^2}, \frac{\Delta_z}{T}\right)\right]$$
$$R_{\perp} = \Delta^2\left[1 + \frac{5\epsilon}{11}\ln\frac{T}{\Delta}\right] + \frac{\epsilon T^2}{11}\left[G\left(\frac{\Delta^2}{T^2}, 0\right) + 4G\left(\frac{\Delta^2}{T^2}, \frac{\Delta_z}{T}\right)\right]. \tag{3.30}$$

The function $G(y, h)$ represents the value of the one-loop momentum integral; it was computed in Refs 29,33 for the zero magnetic field case $h = 0$. The generalization to non-zero h is

$$G(y, h) = -2\int_0^{\infty} dq \left[\ln\left(2q^2\frac{\cosh(\sqrt{q^2 + y}) - \cosh h}{q^2 + y - h^2}\right) - q - \frac{y}{2\sqrt{q^2 + 1/e}}\right] \tag{3.31}$$

This integral has to be evaluated numerically in general, but we have the limiting value $G(0, 0) = 2\pi^2/3$. Stability of the paramagnetic state requires that $m_{\perp} \geq \Delta_z$; this requirement leads to an expression for T_c, which is determined by solving $m_{\perp} = \Delta_z$. Analysis of

this equation in powers of ϵ shows that $T_c \sim 1/\sqrt{\epsilon}$. This implies that $\Delta/T, \Delta_z/T \sim \sqrt{\epsilon}$, and so to leading order we can just use the value of $G(0,0)$ in (3.30) to obtain

$$T_c^2 = \frac{33(\Delta_z^2 - \Delta^2)}{10\pi^2\epsilon} \tag{3.32}$$

for $\Delta_z > \Delta$. For $\Delta_z < \Delta$ the system is in the SS phase, and therefore $T_c = 0$. Notice that (3.32) agrees with the scaling form (3.26). This result is expected to be the leading order result in powers of ϵ, except in the region $|\Delta_z - \Delta| \ll \Delta$ where the ϵ expansion fails and the reduced action $\mathcal{S}_\Psi$ of Section III B 1 has to be used. Using results of Ref 30 for the latter action we have the exact asymptotic form

$$T_c = \frac{(\Delta_z - \Delta)\ln[\Delta_z/(\Delta_z - \Delta)]}{4\ln\ln[\Delta_z/(\Delta_z - \Delta)]} \qquad \text{for } \ln[\Delta_z/(\Delta_z - \Delta)] \gg 1 \tag{3.33}$$

Closely related results can be obtained for $r < 0$. In this case, the masses are universal functions of $\rho_s(0)$, Δ_z and T. However, considerable ambiguity arises in the ϵ expansion for the result because $\rho_s(0)$ does not simply have the dimensions of energy for all d. The appropriate scaling variable[29] is $(\rho_s(0))^{1/(d-1)}$, and it is necessary to keep the full $1/(d-1)$ power, rather than expand it in powers of ϵ in order to make the engineering dimensions of the results come our correct. This then leads to ambiguities as to precisely which numerical factors should be raised to the power $1/(d-1)$ and which to $1/2+\epsilon/4$. A convenient choice, which leads to the most compact expressions is to define

$$\widetilde{\rho_s} \equiv \left(\frac{2\epsilon}{(n+8)}\frac{\rho_s}{S_{d+1}}\right)^{1/(d-1)} \tag{3.34}$$

where we have written the general expression for the n-component order parameter: in the present case $n = 3$. The factor S_{d+1} is a phase-space factor and is given by $S_d = 2/[\Gamma(d/2)(4\pi)^{d/2}]$ (this factor was inadvertently omitted in Ref 29). Notice that $\widetilde{\rho_s}$ has the dimensions of energy in $d = 2$ (which is of interest here). The value of $\widetilde{\rho_s}$, however must be regarded as subject to large systematic corrections, in view of the ambiguities noted above. Using the methods and results of Ref 29 for $r < 0$, and expressing them in terms of $\widetilde{\rho_s}$, we find that the results (3.29) still hold, but (3.30) are replaced by

$$R_{\parallel} = -\frac{\widetilde{\rho}_s^2}{2}\left[1 - \frac{\epsilon}{22} + \frac{5\epsilon}{11}\ln\frac{T}{\widetilde{\rho}_s}\right] + \frac{\epsilon T^2}{11}\left[3G\left(-\frac{\widetilde{\rho}_s^2}{2T^2}, 0\right) + 2G\left(-\frac{\widetilde{\rho}_s^2}{2T^2}, \frac{\Delta_z}{T}\right)\right]$$
$$R_{\perp} = -\frac{\widetilde{\rho}_s^2}{2}\left[1 - \frac{\epsilon}{22} + \frac{5\epsilon}{11}\ln\frac{T}{\widetilde{\rho}_s}\right] + \frac{\epsilon T^2}{11}\left[G\left(-\frac{\widetilde{\rho}_s^2}{2T^2}, 0\right) + 4G\left(-\frac{\widetilde{\rho}_s^2}{2T^2}, \frac{\Delta_z}{T}\right)\right]. \tag{3.35}$$

Notice that $G(y,h)$ is now needed for negative values of y. Despite appearances, the expression (3.31) actually also holds for $y < 0$—one simply uses the identity $\cosh(ix) = \cos(x)$ when the square root becomes purely imaginary. Indeed, it is not difficult to show that the expression in (3.31) is actually analytic for all real $-\infty < y < \infty$ provided $h > 0$. We can use the same stability condition used for $r > 0$ to now obtain the leading order ϵ-expansion result for T_c:

$$T_c^2 = \frac{33(\Delta_z^2 + \widetilde{\rho}_s^2/2)}{10\pi^2\epsilon}, \tag{3.36}$$

which is of the scaling form (3.28). The ϵ expansion fails when $\Delta_z \ll \rho_s(0)$ where the system approaches the C-N phase boundary; here, we use the effective action $\mathcal{S}_n$ of Section III B 2, and results for it in Ref 32 to obtain

$$T_c = \frac{2\pi\rho_s(0)}{\ln(\rho_s(0)/\Delta_z)} \qquad \text{for } \ln(\rho_s(0)/\Delta_z) \gg 1. \tag{3.37}$$

Finally, we obtain the damping coefficients $\Gamma_{\perp,\parallel}$. This requires evaluation of two-loop diagrams and the results are extremely lengthy. We will be satisfied here by simply quoting the results valid for $\Delta_z/T \ll 1$, (Δ or $\rho_s(0)$)$/T \ll 1$ which were obtained in Ref 29:

$$\Gamma_{\perp}(\omega) = \Gamma_{\parallel}(\omega) = \frac{10\pi\epsilon^2}{121}\left(\frac{\omega^2}{8} + \pi^2T^2 + 6T^2\mathrm{Li}_2(e^{-\omega/2T})\right) \tag{3.38}$$

where $\mathrm{Li}_2(x)$ is the dilogarithm function

$$\mathrm{Li}_2(x) = -\int_0^x \frac{dy}{y}\ln(1-y) \tag{3.39}$$

D. Connection to the Hartree-Fock theory

The effective field theory for the double-layer QH system at a filling factor of $\nu = 2/m$ (with m an odd integer) that we develop above is entirely built on the effective action

S_2, defined by Eq. (3.8). In particular, we make use of the fact that this effective action for our problem is identical to the action of the $2+1$ dimensional $O(3)$ quantum nonlinear σ model[26–33] with the additional feature of an external magnetic field coupled to the conserved global $O(3)$ charge. Once this precise mapping of our effective action to that of the $2+1$ dimensional $O(3)$ quantum nonlinear σ model becomes explicit, the rest of the results derived in sections IIIA–C follow naturally. The question now arises about the correspondence between our effective field theory results in this section and the microscopic Hartree-Fock results (for $\nu = 2$) described in sections II A–II C.

It is to be noted that both the microscopic Hartree-Fock theory (sections II A–II C) and the effective nonlinear σ model field theory predict the same number of zero temperature quantum phases, namely the fully spin polarized ferromagnetic, the canted antiferromagnetic, the Néel, and the symmetric spin singlet phase, for the double-layer QH system at $\nu = 2$. (The effective field theory, in addition, enables us to predict that the double-layer system at all fillings $\nu = 2\nu_1$, where $\nu_1 = 1/m$ with m odd, has these four phases with the spin singlet phase in the general case being a non-trivial correlated SS phase rather than just the pseudospin-symmetric spin-antisymmetric SYM phase of the $\nu = 2$ Hartree-Fock theory.) It should also be noted that both the Hartree-Fock theory and the effective field theory predict the existence of a finite temperature Kosterlitz-Thouless phase transition in the canted antiferromagnetic phase with the planar antiferromagnetic ordering disappearing above the Kosterlitz-Thouless transition temperature. The underlying physics in both the theories is that the system is essentially an X–Y antiferromagnet in the layer (i.e. in the plane perpendicular to the magnetic field direction) in the new canted phase.

On a more quantitative level it is easy to show that both theories predict the same topology of the zero temperature quantum phase diagram. This is demonstrated in Fig. 15 where we have redrawn the Hartree-Fock phase diagram (Fig. 15a) of Fig. 10 inverting abscissa (from Δ_{sas}/U_- to U_-/Δ_{sas}) and have somewhat reconfigured the effective field theory phase diagram (Fig. 15b) from Fig. 13 by keeping only the QF_1 phase and by modifying the relative size of the various phases (which are arbitrary within the effective

field theory). Using the definitions $t = (J/\rho_s^o M_o^2)^{1/2}$ from Eq. (3.9) to define the abscissa, the effective field theory phase diagram in $t - \Delta_z$ space (Fig. 15b) can be seen to be identical topologically to the quantitatively calculated Hartree-Fock phase diagram (for $\nu = 2$) in the $\Delta_{sas}/U_- - \Delta_z/\Delta_{sas}$ space (Fig. 10). Note that, in addition to the identical topology involving four distinct quantum phases as shown in Fig. 15 of the two phase diagrams with the effective coupling parameter t of the field theory (the abscissa in Fig. 15b) being proportional to the parameter Δ_{sas}/U_- (the abscissa in Fig. 15a) of the Hartree-Fock theory (which is expected, because $t \sim \Delta_{sas}/U$ with J being the interlayer superexchange coupling) and the ordinate ($\sim \Delta_z$) being the same in both Figs. 15a and 15b, the multicritical point M on the zero magnetic field line shows up in both phase diagrams. At the (zero temperature) quantum multicritical point M, the canted, the spin singlet, and the Néel phase coexist. (The other distinct multicritical point of the Hartree-Fock theory, which is apparent on the abscissa of Fig. 10 where $\Delta_{sas} = \Delta_z$ and $d = 0$, where the ferromagnetic, the canted and the symmetric phase coexist is not accessible within the effective field theory because of its long wavelength approximation, and can not be seen in Fig. 15a as it is pushed to the point $U_-/\Delta_{sas} = 0$, $\Delta_z/\Delta_{\rm sas} = 1$ where the two Hartree-Fock phase boundaries of Fig. 15a come together.) It is, therefore, obvious that, except for very small values of d (where the effective field theory which applies only when $d > l_o$), the quantum phase diagrams predicted by the two theories are topologically identical.

Finally, we can actually estimate the $\nu = 2$ double-layer Kosterlitz-Thouless transition temperature, T_c of section IIIC, in the effective field theory by using the microscopic parameters obtained within the Hartree-Fock theory. This calculation[9], where one incorporate the calculated Hartree-Fock parameters for Δ and $\epsilon = 1$ in Eq. (3.36), leads[37] to an estimated effective field theory $T_c \approx 3K$ which is somewhat larger than the critical temperature T_c (Eq. (2.27)) estimated within the long wavelength mean field Hartree-Fock treatment of section II C. In general, we believe the ϵ–expansion leads substantial overestimates of transition temperatures because it does not properly account for the low-dimensional vortex effects

responsible for the transition.

IV. COMPARISON WITH EXPERIMENTS

In this section, we discuss some recent double-layer $\nu = 2$ inelastic light scattering experiments whose findings are consistent with our theoretical results. A detailed quantitative comparison between our theory and the experiment requires an accurate knowledge of the temperature dependence of the related experimentally relevant response functions as the system undergoes a finite temperature phase transition at T_c. Such a quantitative description is at present lacking, and therefore we restrict ourselves mostly to a qualitative discussion.

In a recent inelastic light scattering experiment,[8] the long wavelength ω_0 mode of the intersubband SDW triplet (see Fig. 16 for schematic details of the various possible SDW modes in the system), which corresponds to transition $|0\sigma\rangle \rightarrow |1\sigma\rangle$, is measured for $\nu = 2$ double-layer quantum Hall systems. The double-layer samples used in the experiment are by design in the canted antiferromagnetic phase according to our zero temperature Hartree-Fock phase diagram, *i.e.,* the ground state of the experimental system is the canted antiferromagnetic quantum Hall state (see Figs. 4, 10, and 15 for the location of the experimental sample in our theoretical diagram). The experiment[8] shows two important and striking features: One is that there is a threshold temperature ($\sim 0.5K$) below which the ω_0 mode becomes unobservable as it seems to lose all spectral weight, the other feature is that the excitation energy ω_0 approaches the Zeeman energy Δ_z when the threshold temperature is approached from the above, *i.e.* $\omega_0 \approx \Delta_z$. We argue below that these experimental observations are completely consistent with our predicted Kosterlitz-Thouless transition in the canted antiferromagnetic phase being the observed experimental transition at T_c.

First, we notice that the ω_0 mode, which involves a no-spin-flip transition with $\delta S_z = 0$, has a maximum spectral weight in the symmetric phase, where there are as many spin-up (down) empty states as there are spin-up (down) electrons. The spectral weight of the ω_0 mode is identically zero in the ferromagnetic phase, where all spin-up states are occupied

and all empty states are spin-down, and hence the ω_0 mode (which does not involve any spin flip) is forbidden. The spectral weight of the ω_0 mode should be nonzero but small in the antiferromagnetic phase. This is because the canted antiferromagnetic phase lies between the symmetric phase and the ferromagnetic phase in the phase diagram and its spin-flip dynamics should thus be intermediate. More over, the canted antiferromagnetic phase is not an eigenstate for either spin or pseudospin, so the small spectral weight of the ω_0 mode is shared by many allowed transitions, spreading the mode intensity over these transitions and thus making the spectral weight of each transition even smaller. It is thus plausible to regard the observed disappearance of the ω_0 mode at the threshold temperature as the transition to the canted antiferromagnetic phase at lower temperatures (where the spectral intensity for the ω_0 mode becomes very small). Above the transition temperature the system is essentially a disordered planar X-Y magnet, and thus behaves like a paramagnet whose SDW properties should be very similar to the paramagnetic spin-singlet symmetric phase.

Next, we notice that, in the symmetric phase, the excitation energies of the intersubband SDW triplet have the following simple relationship

$$\omega_{\pm} = \omega_0 \pm \Delta_z. \tag{4.1}$$

This expression can be derived explicitly, using either the diagrammatic time-dependent Hartree-Fock approximation or the single-mode approximation. It is a direct consequence of the fact that Coulomb interaction is spin independent. The above relationship bears a clear physical meaning: $\omega_0 \to \Delta_z$ means that $\omega_- \to 0$, *i.e.* mode softening (see Fig. 16). Thus, the experimental observation that ω_0 approaches the Zeeman energy as the threshold temperature is reached from above suggests that there is mode softening ($\omega_- = 0$) at the phase boundary, as predicted by the computations of the T-dependent peak positions in Section III C.

Finally, we note that the critical temperature (the threshold temperature) in the experiment[8] is $T_c \approx 0.52K$, which is reasonably close to our calculated Kosterlitz–Thouless critical temperature $T_c \approx 1.8K$ in the Hartree-Fock theory (Eq. (2.27)) using the ac-

tual experimental sample parameters.[9] This discrepancy between the experiment and the Hartree-Fock theory is small when compared with the energy scale of Coulomb interaction, which is about $70K$ in this particular sample. In addition, quantum fluctuations neglected in the Hartree-Fock theory should lower the calculated critical temperature and reduce this discrepancy.

From the above discussions, we conclude that our theoretical predictions are consistent with the recent light scattering experimental results. The most dramatic aspect of the experimental observations which give us confidence in believing that the experiment is really seeing the canted antiferromagnetic phase are (i) the unambiguous observation of a mode softening (*i.e.* $\omega_0 \rightarrow \Delta_z$ implying $\omega_- \rightarrow 0$); (ii) the observed temperature dependence indicating a finite temperature phase transition; (iii) the location of the experimental sample in our calculated phase diagram and (iv) the $\omega_0 \rightarrow \Delta_z$ collapse being observed precisely at $\nu = 2$.

While the recent inelastic light scattering experiment[8] provides, in our opinion, rather compelling evidence in favor of there being a finite temperature (Kosterlitz-Thouless) transition in the $\nu = 2$ double-layer system with the low temperature phase being the canted antiferromagnetic phase (by virtue of the vanishing of the ω_- mode at the phase boundary, as discussed in section II B of this article), a complete verification of our theory awaits further more conclusive and direct experimental measurements, especially heat capacity measurements which should shown (Fig. 12) power law temperature dependence in the canted phase due to the existence of the Goldstone mode and exponential temperature dependence in the two normal phases due to the existence of gaps in the excitation spectra, would be particularly well-suited in verifying our phase diagram. The direct observation of a gapless Goldstone mode (Fig. 9) in the inelastic light scattering measurement in the (low temperature) canted phase would also be rather definitive in establishing the existence of the canted phase. In this context we mention that the SDW softening indicating a phase transition to the canted phase is a long wavelength instability, and therefore optical spectroscopy[41] may also be useful in studying our proposed $\nu = 2$ double-layer phase diagram. Both of these pro-

posed direct experiments are fraught with considerable (experimental) difficulties, however. Electronic heat capacity measurements in quantum well structures are notoriously difficult by virtue of the extremely small magnitude of the (2D) electronic heat capacity compared with the background (lattice) contribution. As for the direct experimental observation of the Goldstone mode, the experimental inelastic light scattering spectroscopy is severely restricted by the selection rules inherent in the resonant light scattering spectroscopy, and at this stage it is unclear whether the problems associated with the selection rules would allow to directly observe the Goldstone mode.

One striking difference between the physics of $\nu = 2$ double-layer system and the corresponding $\nu = 1$ situation is the existence of a charge gap in the $\nu = 2$ case for all values of d and $\Delta_{\rm sas}$: the system is always incompressible (in all its quantum phases including the canted phase). Thus the quantized Hall effect exists throughout our phase diagram unlike in the corresponding $\nu = 1$ situation.[3,4,12,42] The existence/nonexistence of the QH effect, which has been useful in mapping out the $\nu = 1$ double-layer phase diagram[42] would not work in our problem in a direct sense. We do, however, speculate that the activation energy (*i.e.* the effective value of the incompressible charge gap) for the $\nu = 2\nu_1$ double-layer QH effect may very well show observable structure at our calculated phase boundaries even though all the phases (ferromagnetic, canted, symmetric) would exhibit $\nu = 2\nu_1$ QH effect. We suggest systematic experimental investigations of $\nu = 2\nu_1$ double-layer ($\nu_1 = 1/m$ with $m = 1, 3, 5, ...$) QH activation energies by tuning $\Delta_{\rm sas}$, Δ_z, and d to look for signatures of our proposed zero and finite temperature phase transitions.

In this context we point out that there is already some experimental evidence[38,39] that the naive $\Delta_z = \Delta_{\rm sas}$ level crossing in $\nu = 2$ double-layer QH systems does not exist (as our theory proposes and clearly demonstrates in our calculated phase diagrams). The experimental observation[38,39] has been that the naive $\nu = 2$ level crossing phenomenon (at $\Delta_z = \Delta_{\rm sas}$) between ferromagnetic and symmetric phases, which would exist in the absence of our intervening canted phase, if it happens at all in double-layer systems, must happen at magnetic fields *much lower* than that satisfying $\Delta_z = \Delta_{\rm sas}$ condition. This is, of course,

exactly what our phase diagram (see Fig. 4)) predicts — nothing interesting happens for finite d at $\Delta_z = \Delta_{\rm sas}$ or for that matter even for $\Delta_{\rm sas} = 3\Delta_z$ at $d = 2l_o$ in Fig. 4a for example— the system remains in the fully spin polarized ferromagnetic phase and the naive expectation of a level crossing transition to the symmetric phase simply does not occur. In this sense, our phase diagram for the $\nu = 2$ double-layer system may have already been verified in 1990![42] Further experiments along this line at $\nu = 2\nu_1$ double-layer systems would be useful.

V. SUMMARY

In summary, we have studied both zero and finite temperature properties of the $\nu = 2$ double-layer QH systems within the framework of Hartree-Fock approximation. We show that, in addition to the fully polarized state adiabatically connected to the well separated layer state, there are two other double-layer quantum Hall phases: the first is a spin singlet, and the second is characterized by a finite interlayer inplane canted antiferromagnetic spin ordering. The transition between the different quantum Hall phases is continuous, and is signaled by the softening of collective intersubband spin density excitations. Because of the broken $U(1)$ symmetry in the canted antiferromagnetic phase, the system has a finite temperature Kosterlitz-Thouless transition ($T_c \sim 1K$). Below the critical temperature, the canted antiferromagnetic phase supports a linear Goldstone mode. Above, the system is essentially a paramagnet similar to the symmetric phase. Our findings are consistent with recent light scattering spectroscopic experimental results. We present detailed results of our study, including the stability energetics of various phases, the antiferromagnetic order parameter in the canted phase, the phase diagram, the collective excitation dispersions, the specific heat, and the Kosterlitz-Thouless critical temperature, and suggest various experiments which could, in principle, probe the rich double-layer phase diagram predicted by our theory.

In addition to the microscopic $\nu = 2$ Hartree-Fock theory, we have developed a rather

general long wavelength effective field theory for the $\nu = 2\nu_1$, where $\nu_1 = 1/m$ with m an odd integer, double-layer system. The essential inputs for this effective field theory are the existence of charge gaps in the two layers and an effective interlayer antiferromagnetic (superexchange) interaction. By mapping the effective action for this problem to that of an $O(3)$ quantum nonlinear σ model, we have been able to show that the qualitative phase diagram calculated within the Hartree-Fock theory for $\nu = 2$ is actually generically valid (topologically) for any $\nu = 2\nu_1$ (with $\nu_1 = 1, 1/3, 1/5, ...$) double-layer system with the symmetric phase of the Hartree-Fock calculation being replaced by a highly non-trivial correlated spin singlet phase (of which the $\nu = 2$ symmetric phase is a rather trivial example). Thus, there could be rather non-trivial canted (and perhaps even Néel, if one can apply sufficient external pressure to produce vanishing gyromagnetic ratio) antiferromagnets at, for example, $\nu = 2/3$ in a double-layer system, where each single fully spin polarized Laughlin state spontaneously develops in-plane antiferromagnetic spin ordering. Observation of the canted or the spin-singlet phase in a $\nu = 2/3$ double-layer QH system would significantly enrich the many-body strong correlation physics associated with QH systems.

We conclude by pointing out that, although we have confined ourselves in this article to the $\nu = 2/m$ case, with m an odd integer, it is obvious that the physics we are considering here applies, in principle, to all double-layer QH systems with $\nu = 2\nu_1$ where a single layer at filling ν_1 forms a fully *spin polarized* incompressible QH state with a charge gap. Thus, the same physics as at $\nu = 2$ should apply, in principle, at $\nu = 6$ (but *not* at $\nu = 4, 8, ...$ where the charge gap is the cyclotron gap not $\Delta_z, \Delta_{\rm sas}$.) in double-layer system. In principle, however, our approximations which neglect all (orbital) Landau level couplings become progressively worse at higher Landau levels. In this respect, it is very gratifying that the experimental light scattering measurements[8] find qualitatively similar (but quantitatively much suppressed) behavior at $\nu = 6$ as at $\nu = 2$, but the $\nu = 4$ situation is qualitatively different.

ACKNOWLEDGMENTS

The authors thank Dr. A. Pinczuk and Dr. V. Pellegrini for helpful discussions on the experimental data. The work at University of Maryland is supported by the U.S.-ONR and the U.S.-ARO. The work at Yale University is supported by NSF Grant No DMR 96-23181.

APPENDIX A: TWO SPIN PROBLEM

Here we will assess the validity of the mapping from the action $\mathcal{S}_1$ in (3.4) to $\mathcal{S}_2$ in (3.8) by examining a simple toy model of two spins. We consider the Hamiltonian

$$\mathcal{H} = J\vec{S}_1 \cdot \vec{S}_2 - \Delta_z \hat{z} \cdot (\vec{S}_1 + \vec{S}_2) \tag{A1}$$

where $\vec{S}_{1,2}$ are two quantum spins of spin S. The energy spectrum of $\mathcal{B}$ is clearly

$$E_\ell = \frac{J}{2}\ell(\ell+1) - \Delta_z m + E_0 \qquad , \qquad \ell = 0, 1, \ldots 2S \;\; ; \;\; m = -\ell, -\ell+1, \ldots \ell-1, \ell \tag{A2}$$

where E_0 is an overall constant we shall not be interested in.

Let us attempt to obtain this result using the coherent state path integral. First, we transcribe $\mathcal{H}$ into the effective action

$$\mathcal{S} = \int d\tau \left[iS\vec{A}(\vec{n_1}) \cdot \frac{\partial \vec{n_1}}{\partial \tau} + iS\vec{A}(\vec{n_2}) \cdot \frac{\partial \vec{n_2}}{\partial \tau} + JS^2 \vec{n}_1 \cdot \vec{n}_2 \right] \tag{A3}$$

where $\vec{n}_{1,2}^2 = 1$. Notice that this is the analog of the action $\mathcal{S}_1$ in (3.4) with only the spatial gradient spin stiffness terms now being absent. Now insert the parameterization (3.5) into (A3), and expand to quadratic order in $\vec{L}$. The neglect of terms higher order in $\vec{L}$ is the only approximation being made here. This gives us the analog of (3.7)

$$\mathcal{S} \approx \int d\tau \left[2iS\vec{L} \cdot \left(\vec{n} \times \frac{\partial \vec{n}}{\partial \tau} + i\Delta_z \hat{z} \right) + 2J\vec{L}^2 \right] \tag{A4}$$

Now we integrate out $\vec{L}$ as described above (3.8) to obtain

$$\mathcal{S} \approx \int d\tau \frac{1}{2J} \left(\frac{\partial \vec{n}}{\partial \tau} - i\Delta_z \hat{z} \times \vec{n} \right)^2 \tag{A5}$$

where recall that the functional integral is over the unit vector field $\vec{n}(\tau)$ satisfying $\vec{n}^2 = 1$ for all τ. This last form of $\mathcal{S}$ is the effective action for a quantum rotor in a field $\Delta_z \hat{z}$. This action is equivalent to the Hamiltonian

$$\mathcal{H}_R = \frac{J}{2}\hat{\vec{L}}^2 - \Delta_z \hat{z} \cdot \hat{\vec{L}} \tag{A6}$$

where $\hat{\vec{L}}$ is the rotor angular momentum operator. The eigenvalues of $\mathcal{H}_R$ are easily seen to be identical to those of $\mathcal{H}$ in (A2) with one simple difference. The allowed values of ℓ now extend over *all* non-negative integers. Thus the only effect of dropping terms higher order in $\vec{L}$ in the functional analysis is that the upper bound $\ell \leq 2S$ has disappeared. This only introduces additional states at relatively high energies and is therefore not expected to be of importance in our study of the low energy properties of $\mathcal{S}_2$.

REFERENCES

[1] *Quantum Hall Effect*, edited by R.E. Prange and S.M. Girvin (Springer-Verlag, New York, 1987); *Perspectives in Quantum Hall Effects*, edited by S. Das Sarma and A. Pinczuk (Wiley, New York, 1997).

[2] S.Q. Murphy J.P. Eisenstein, G.S. Boebinger, L.N. Pfeiffer, and K.W. West, Phys. Rev. Lett. **72**, 728 (1994)

[3] K. Yang, K. Moon, L. Zheng, A.H. MacDonald, S.M. Girvin, D. Yoshioka, and Shou-Cheng Zhang, Phys. Rev. Lett. **72**, 732 (1994); X.G. Wen and A. Zee, Phys. Rev. Lett. **69**, 1811 (1992); Z.F. Ezawa and A. Iwazaki, Phys. Rev. B **47**, 7295 (1993).

[4] K. Moon, H. Mori, Kun Yang, S.M. Girvin, A.H. MacDonald, L. Zheng, D. Yoshioka, and Shou-Cheng Zhang, Phys. Rev. B **51**, 5138 (1995).

[5] Y.W. Suen, L.W. Engel, M.B. Santos, M. Shayegan, and D.C. Tsui , Phys. Rev. Lett. **68**, 1379 (1992); J.P. Eisenstein, G.S. Boebinger, L.N. Pfeiffer, K.W. West, and Song He, *ibid.* **68**, 1383 (1992); D. Yoshioka, A.H. MacDonald, and S.M. Girvin, Phys. Rev. B **39**, 1932 (1989); Song He, S. Das Sarma, and X.C. Xie, *ibid.* **47**, 4394 (1993).

[6] S. Das Sarma and P.I. Tamborenea, Phys. Rev. Lett. **73**, 1971 (1994); R.J. Radtke, P.I. Tamborenea, and S. Das Sarma, Phys. Rev. B **54**, 13832 (1996).

[7] Lian Zheng, R.J. Radtke, and S.. Das Sarma, Phys. Rev. Lett. **78**, 2453 (1997).

[8] V. Pellegrini, A. Pinczuk, B.S. Dennis, A.S. Plaut, L.N. Pfeiffer, and K.W. West, Phys. Rev. Lett. **78**, 310 (1997).

[9] S. Das Sarma, S. Sachdev, and L. Zheng, Phys. Rev. Lett. **79**, 917 (1997).

[10] R. Côté, L. Brey, and A.H. MacDonald, Phys. Rev. B **46**, 10239 (1992); L. Zheng and H.A. Fertig, *ibid.* **52**, 12282 (1995).

[11] Y.A. Bychkov, S.V. Iordanskii and G.M. Eliashberg, JETP Lett. **33**, 143 (1981); C. Kallin

and B.I. Halperin, Phys. Rev. B **30**, 5655 (1984).

[12] A.H. MacDonald, P.M. Platzman, and G.S. Boebinger, Phys. Rev. Lett. **65**, 775 (1990); L. Brey, *ibid.* **65**, 903 (1990); H.A. Fertig, Phys. Rev. B **40**, 1087 (1989); X.M. Chen and J.J. Quinn, *ibid.* **45**, 11054 (1992); G.S. Boebinger, H.W. Jiang, L.N. Pfeiffer, and K.W. West, Phys. Rev. Lett. **64**, 1793 (1990).

[13] A. Pinczuk, B.S. Dennis, D. Heiman, C. Kallin, L. Brey, C. Tejedor, S. Schmitt-Rink, L.N. Pfeiffer, and K.W. West, Phys. Rev. Lett. **68**, 3623 (1992).

[14] The finite well-thickness corrections, as well as other detailed corrections to interaction potentials, have quantitative effects only. They do not change any results qualitatively.

[15] A.H. MacDonald, J. Phys. C **18** 1003 (1985).

[16] For notational clarity, we use μ for the subband index, L (R) for the layer index, σ for the electron spin, α for the intra-Landau level index, and $i\lambda$ ($i = 1, 2$ and $\lambda = \pm$) for the four Hartree-Fock eigenstates.

[17] G.D. Mahan, *Many-Particle Physics* (Plenum, New York, 1981); A.L. Fetter and J.D. Walecka, *Quantum Theory of Many-Particle Systems* (McGraw-Hill, New York, 1971).

[18] J.M. Kosterlitz and D.J. Thouless, J. Phys. C **6**, 1181 (1993); J.M. Kosterlitz, *ibid.* **7**, 1046 (1974).

[19] J. Tobochnik and G.V. Chester, Phys. Rev. B **20**, 3761 (1979); J. Fernandez, M.F. Ferreira, and J. Stankiewicz, *ibid.* **34**, 292 (1986); R. Gupta, J. DeLapp, G.G. Batrouni, G.C. Fox, C.F. Baillie, and J. Apostolakis, Phys. Rev. Lett. **61**, 1996 (1988).

[20] V. Bayot, E. Grivei, S. Melinte, M.B. Santos, and M. Shayegan, Phys. Rev. Lett. **76**, 4584 (1996).

[21] D.H. Lee and C.L. Kane, Phys. Rev. Lett. **64**, 1313 (1990)

[22] S.L. Sondhi, A. Karlhede, S.A. Kivelson, and E.H. Rezayi, Phys. Rev. B **47**, 16419 (1993).

[23] H.A. Fertig, L. Brey, R. Côté, and A.H. MacDonald, Phys. Rev. B **50**, 11018 (1994).

[24] N. Read and S. Sachdev, Phys. Rev. Lett. **75**, 3509 (1995).

[25] A.W. Sandvik, A.V. Chubukov, and S. Sachdev, Phys. Rev B, **51**, 16483 (1995).

[26] S. Sachdev, Z. Phys. B **94**, 469 (1994).

[27] S. Sachdev and T. Senthil, Annals of Phys. **251**, 76 (1996).

[28] A.V. Chubukov, S. Sachdev and J. Ye, Phys. Rev. B **49**, 11919 (1994).

[29] S. Sachdev, Phys. Rev. B **55**, 142 (1997); A factor of S_{d+1} has been inadvertently omitted from the expressions for N_0^2 and ρ_s in this paper. This omission also infected Eqn (6) in Ref 9. The present paper contains corrected expressions.

[30] V.N. Popov, Teor. Mat. Phys. **11**, 354 (1972); D.S. Fisher and P.C. Hohenberg, Phys. Rev. B **37**, 4936 (1988).

[31] A.W. Sandvik and D.J. Scalapino Phys. Rev. Lett. **72**, 2777 (1994).

[32] D.R. Nelson and R.A. Pelcovits, Phys. Rev. B. **16**, 2191 (1977).

[33] K. Damle and S. Sachdev, Phys. Rev. B **56**, 8714 (1997).

[34] S. Sachdev, T. Senthil and R. Shankar, Phys. Rev. B **50**, 258 (1994).

[35] M. Stone, Phys. Rev. B **53**, 16573 (1996).

[36] *A Quantum-critical Trio*, by S. Sachdev in *Strongly Correlated Magnetic and Superconducting Systems*, edited by G. Sierra and M. A. Martin-Delgado, Springer Verlag, Berlin (1997).

[37] The estimate of T_c towards the conclusion of Ref 9 is in error because of the omission noted in 29.

[38] J.P. Eisenstein, private communication.

[39] G. Boebinger, unpublished.

[40] S. L. Sondhi, S.M. Girvin, J.P. Carini, and D. Shahar, Rev. Mod. Phys. **69**, 315 (1997).

[41] E.H. Aifer, B.B Goldberg, and D.A. Broido, Phys. Rev. Lett. **76**, 680 (1996).

[42] G.S. Boebinger, H.W. Jiang, L.N. Pfeiffer, and K.W. West, Phys. Rev. Lett. **64**, 1793 (1990).

FIGURES

FIG. 1. The energy per magnetic flux in the symmetric (SYM) state, the spin polarized ferromagnetic (FM) state, and the canted antiferromagnetic (C) state for a $\nu = 2$ double-layer system with $\Delta_{\rm sas} = 0.07e^2/\epsilon l_o$, $\Delta_z = 0.01e^2/\epsilon l_o$, and the well-thickness $d_w = 0.8l_o$.

FIG. 2. Schematic display of electron spin orientations in the canted antiferromagnetic quantum Hall phase.

FIG. 3. The canted antiferromagnetic order parameter versus layer separation for the indicated tunneling and Zeeman energies. The well-thickness $d = 0.8l_o$.

FIG. 4. The zero temperature phase diagrams at $\nu = 2$ within the Hartree-Fock approximation at two different values of the Zeeman energy: (a) $\Delta_z = 0.01e^2/\epsilon l_o$ and (b) $\Delta_z = 0.01e^2/\epsilon l_o$. The quantum well thickness is $d_w = 0.8l_o$ for both the figures. Three phases are present: the symmetric phase (SYM), the spin polarized ferromagnetic phase (FM), and the canted antiferromagnetic phase (C). The '+' in (a) denotes the experimental sample parameters of Ref. 8. The vertical dotted line in each figure indicated the $\Delta_z = \Delta_{\rm sas}$ condition, which is the naive phase boundary between the FM ($\Delta_z > \Delta_{\rm sas}$) and the SYM ($\Delta_z < \Delta_{\rm sas}$) phase with an expected level crossing at $\Delta_z = \Delta_{\rm sas}$.

FIG. 5. Feynman diagram for the intersubband spin density response function in the time-dependent Hartree-Fock approximation, where solid lines are the self-consistent Hartree-Fock electron Greens functions and wiggled lines are Coulomb interaction potentials.

FIG. 6. The inter-subband SDW dispersion $\omega_{\pm}(q)$ in the spin polarized ferromagnetic (FM) phase at $\nu = 2$ with tunneling energy $\Delta_{\rm sas} = 0.02e^2/\epsilon l_o$, Zeeman energy $\Delta_z = 0.01e^2/\epsilon l_o$, layer separation $d = 1.15l_o$, and the well-thickness $d_w = 0.8l_o$.

FIG. 7. The inter-subband SDW dispersion $\omega_{\pm}(q)$ in the symmetric (SYM) phase at $\nu = 2$ with layer separation $d = 0.85l_o$, Zeeman energy $\Delta_z = 0.08e^2/\epsilon l_o$, tunneling energy $\Delta_{\rm sas} = 0.35e^2/\epsilon l_o$, and the well-thickness $d_w = 0.8l_o$.

FIG. 8. The low energy intersubband SDW mode $\omega_-(q=0)$ and the canted antiferromagnetic order parameter (COP) versus tunneling energy with layer separation $d = 1.0l_o$, Zeeman energy $\Delta_z = 0.08e^2/\epsilon l_o$, and the well-thickness $d_w = 0.8l_o$.

FIG. 9. The inter-subband SDW dispersion $\omega_\pm(q)$ in the canted antiferromagnetic (C) phase at $\nu = 2$ with layer separation $d = 1.15l_o$, tunneling energy $\Delta_{\rm sas} = 0.14e^2/\epsilon l_o$, Zeeman energy $\Delta_z = 0.01e^2/\epsilon l_o$, and the well-thickness $d_w = 0.8l_o$.

FIG. 10. Zero temperature phase diagram of a $\nu = 2$ double-layer quantum Hall system within the Hartree-Fock approximation. The phase diagram is expressed in terms of scaled dimensionless variables. The '+' mark represents the experimental sample of Ref. 8. The Néel phase (N) at $\Delta_z = 0$ and $\Delta_{\rm sas} < 2U_-$ is represented by the thick line. The M-point represents the quantum critical point at $\Delta_z = 0$.

FIG. 11. The calculated Kosterlitz–Thouless critical temperature T_c versus tunneling energy $\Delta_{\rm sas}$ at different interlayer separations: dotted line $d = 1.4\ l_o$, solid line $d = 1.2\ l_o$, and dashed line $d = 1.0\ l_o$. Zeeman energy $\Delta_z = 0.04\ e^2/\epsilon l_o$. The layer-thickness $d_w = 0.8\ l_o$.

FIG. 12. The heat capacity per magnetic flux of a $\nu = 2$ double-layer quantum Hall system as functions of temperature in the symmetry phase (SYM), in the spin-polarized ferromagnetic phase (FM), and in the canted antiferromagnetic phase (C). The inset shows $C/\mathcal{T}^2$, where $\mathcal{T} = k_B T/(e^2/\epsilon l_o)$, versus T in the C phase.

FIG. 13. Mean field phase diagram of the quantum rotor Hamiltonian $\mathcal{H}$ in (3.10). The phases are described in Section III A. Only the QF_1 phase is expected to appear for the two-layer model under consideration here, and is referred to elsewhere as the FM: the QF_2 phase is an artifact of the approximations made in deriving the rotor model. The SS phase was also called the SYM phase in the Hartree Fock computations.

FIG. 14. Mean field phase diagram of the soft-spin action $\mathcal{S}_\phi$ in (3.14). The SS phase was also called the SYM phase in the Hartree Fock computations. Notice that it captures the vicinity of the point M in the rotor mean field phase diagram in Fig 13. The multicritical point M is described by a relativistic continuum field theory with dynamic exponent $z = 1$. The SS-C boundary is a line of second order transitions with dynamic exponent $z = 2$ and is described by action $\mathcal{S}_\Psi$ in (3.24). The position of this boundary is given exactly by $\Delta = \Delta_z$, where $\Delta \sim r^\nu$ is the $\Delta_z = 0$ spin gap of the SS phase (ν is the correlation length exponent of M). The action $\mathcal{S}_\Psi$ holds for $|\Delta - \Delta_z| \ll \Delta$. The N state has $T = 0$ spin stiffness $\rho_s(0) \sim (-r)^\nu$, and for $\Delta_z \ll \rho_s(0)$, the action $\mathcal{S}_n$ in (3.25) describes low T fluctuations.

FIG. 15. (a) The Zero temperature phase diagram of a double-layer quantum Hall system at $\nu = 2$ within the Hartree-Fock approximation. This is the same diagram as Fig. 10. It is redrawn here with the abscissa inverted. The '+' mark represents the experimental sample of Ref. 8. The Néel phase (N) at $\Delta_z = 0$ and $\Delta_{\rm sas} < 2U_-$ is represented by the thick line. (b) Zero temperature phase diagram of a double-layer quantum Hall system at $\nu = 2\nu_1$ derived from the effective Lagrangean $\mathcal{S}_2$ (Eq. (3.8)). The inset shows the topologically identical Hartree-Fock phase diagram of Fig. 10. The FPF, C, and SS phases in the main figure correspond to the FM, AF, and SYM phases in the inset, respectively.

FIG. 16. The intersubband spin excitation transitions in a double-layer quantum Hall system at $\nu = 2$ in the (a) symmetric phase, (b) ferromagnetic phase, and (c) the canted antiferromagnetic phase. The spin conserved transition (ω_0 mode) has large spectral weight in the symmetric phase and is prohibited in the ferromagnetic phase.

Fig1 Zheng, Das Sarma, Sachdev

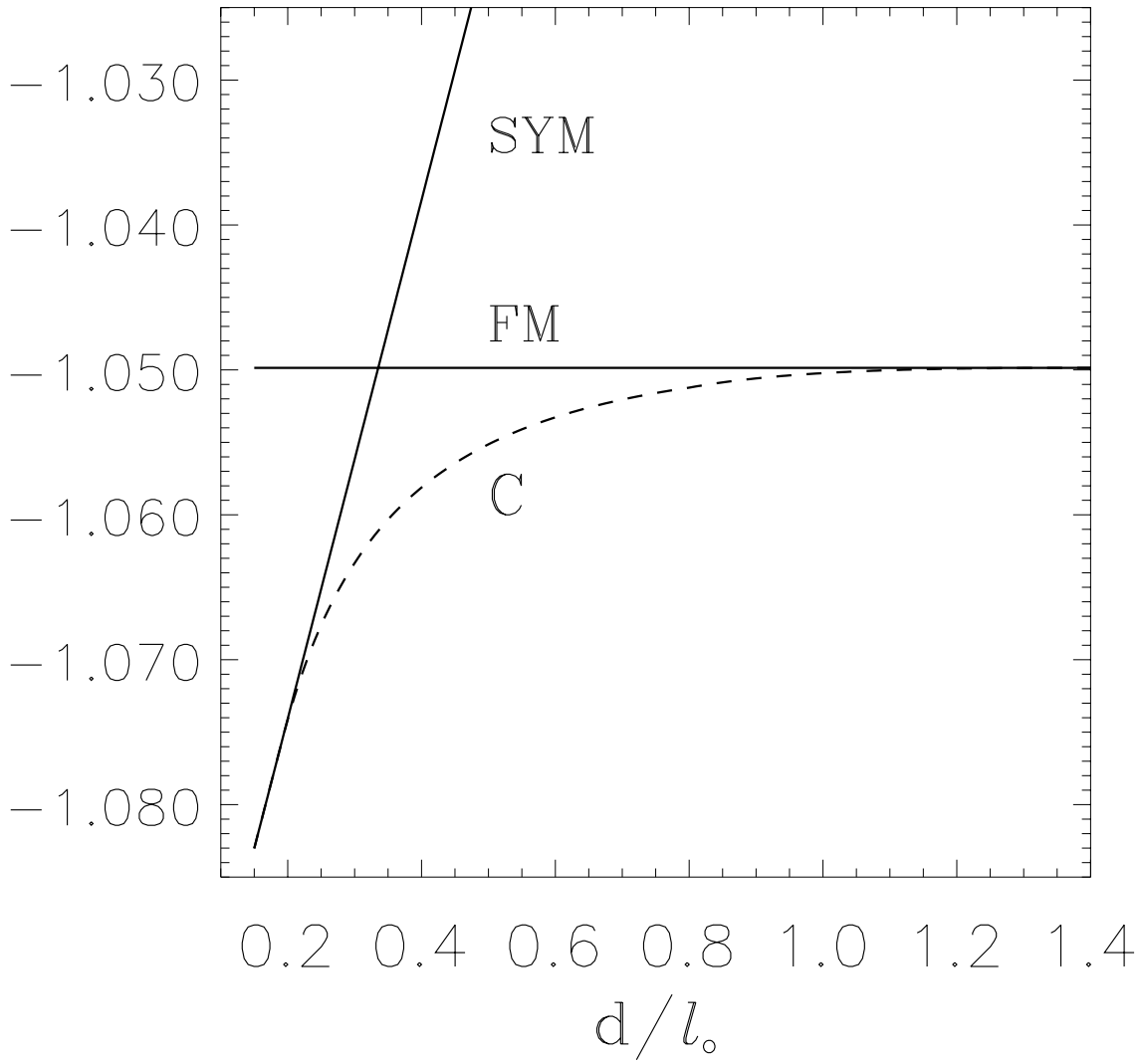

Fig 2 Zheng, Das Sarma, Sachdev

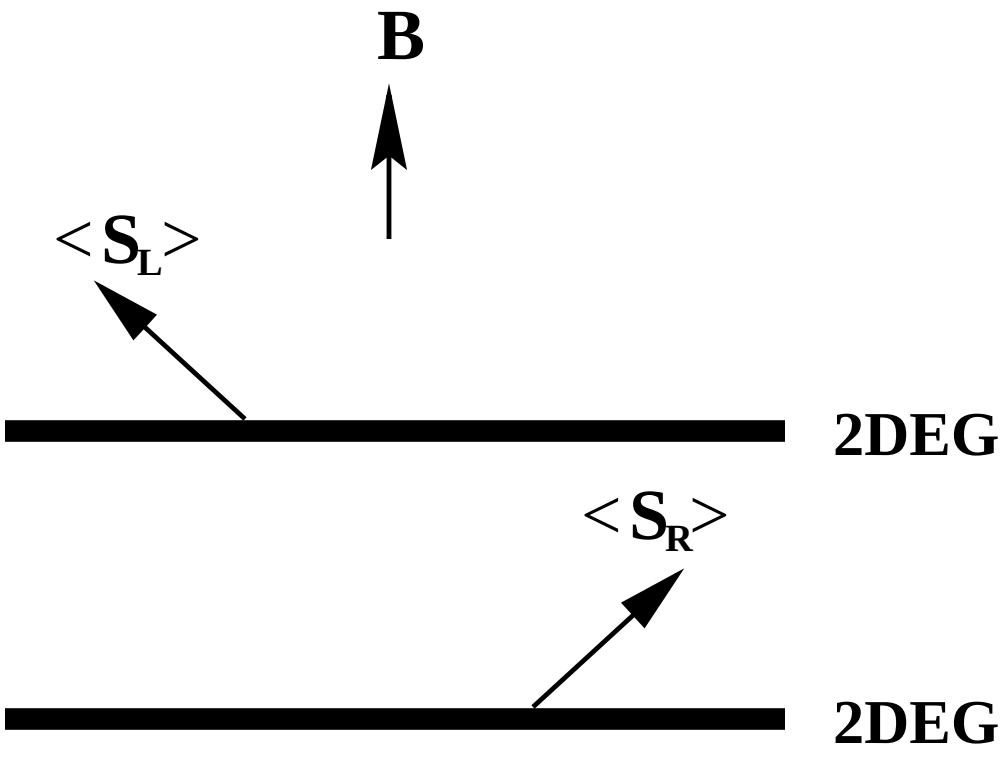

Fig3 Zheng, Das Sarma, Sachdev

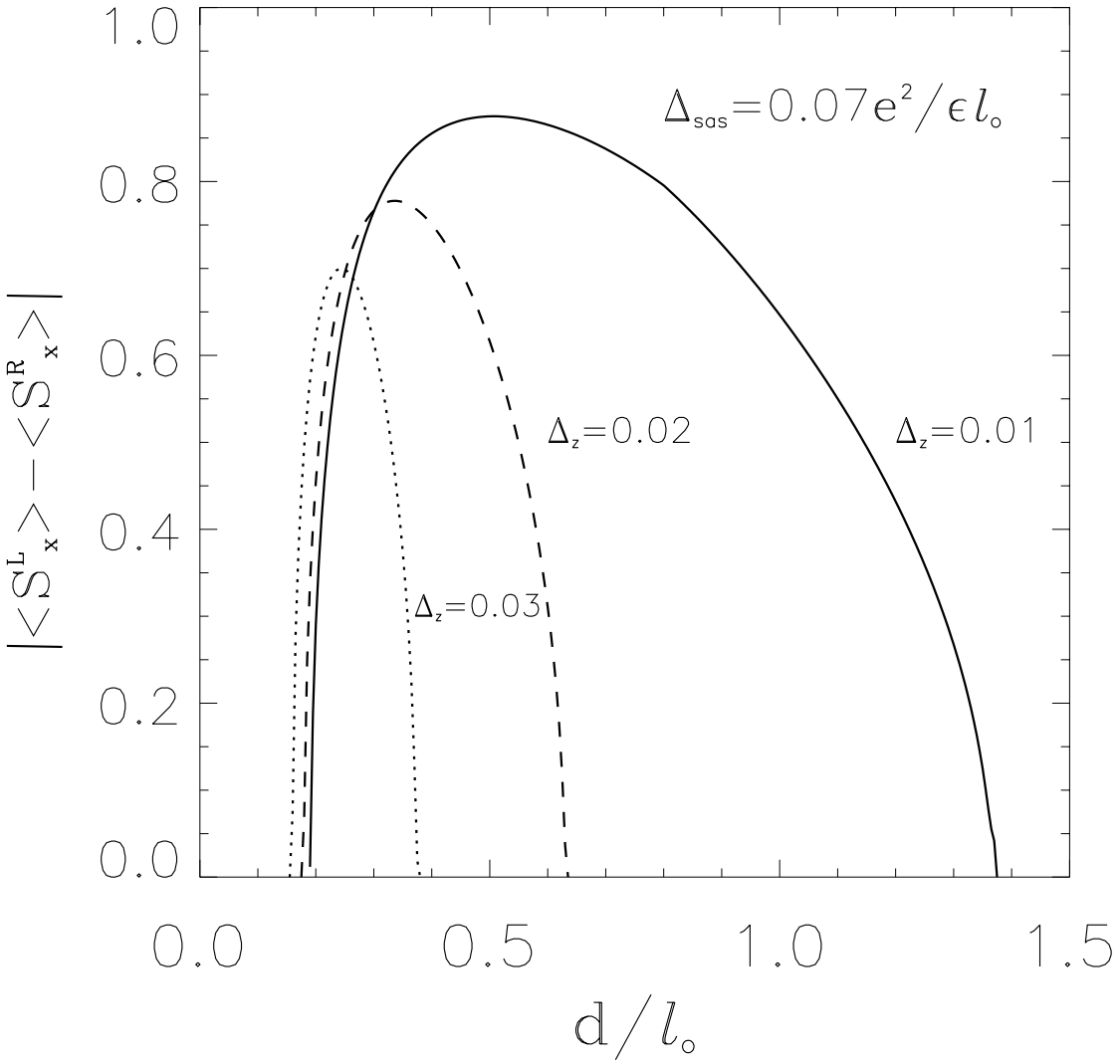

Fig4a Zheng, Das Sarma, Sachdev

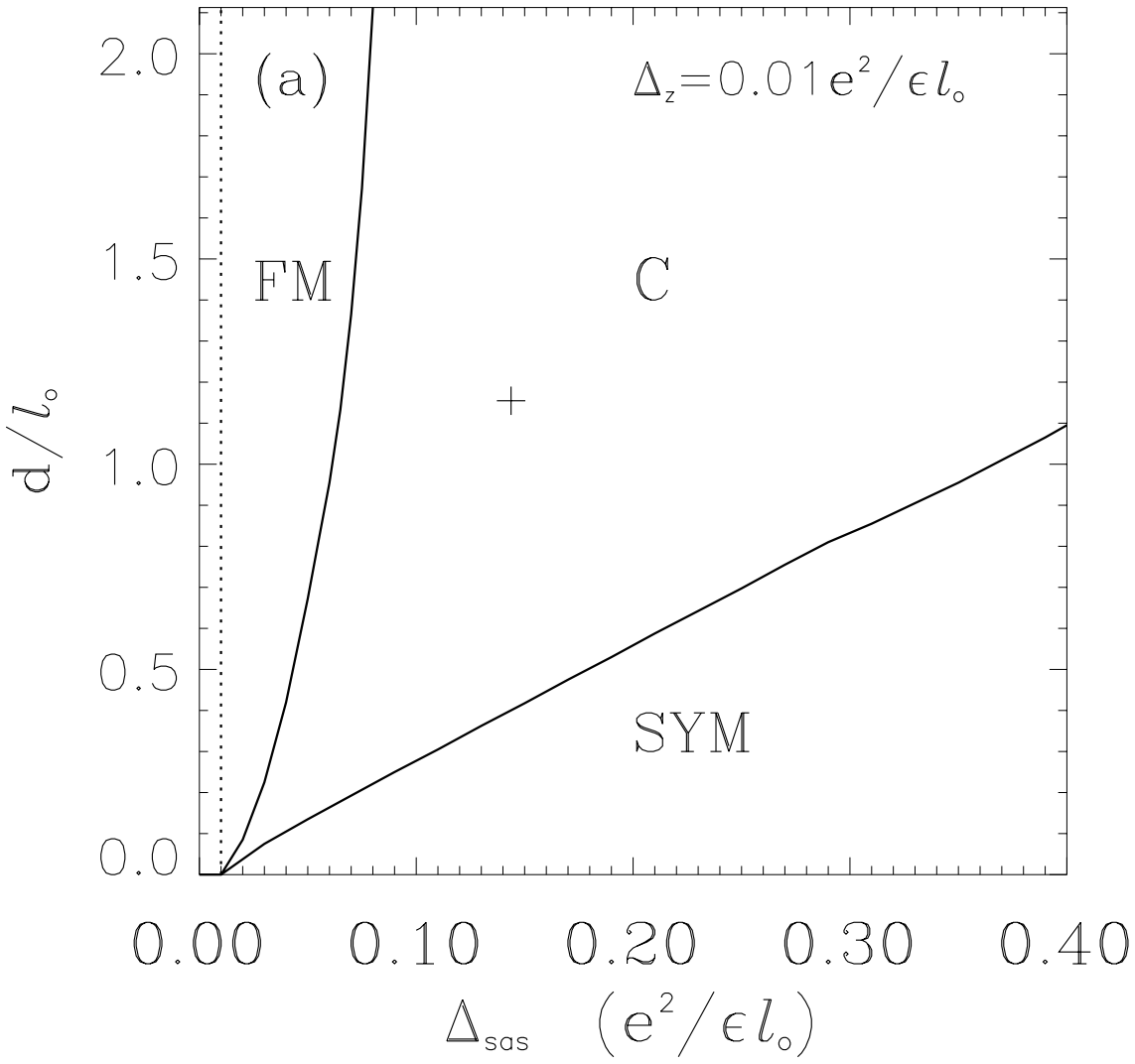

Fig4b Zheng, Das Sarma, Sachdev

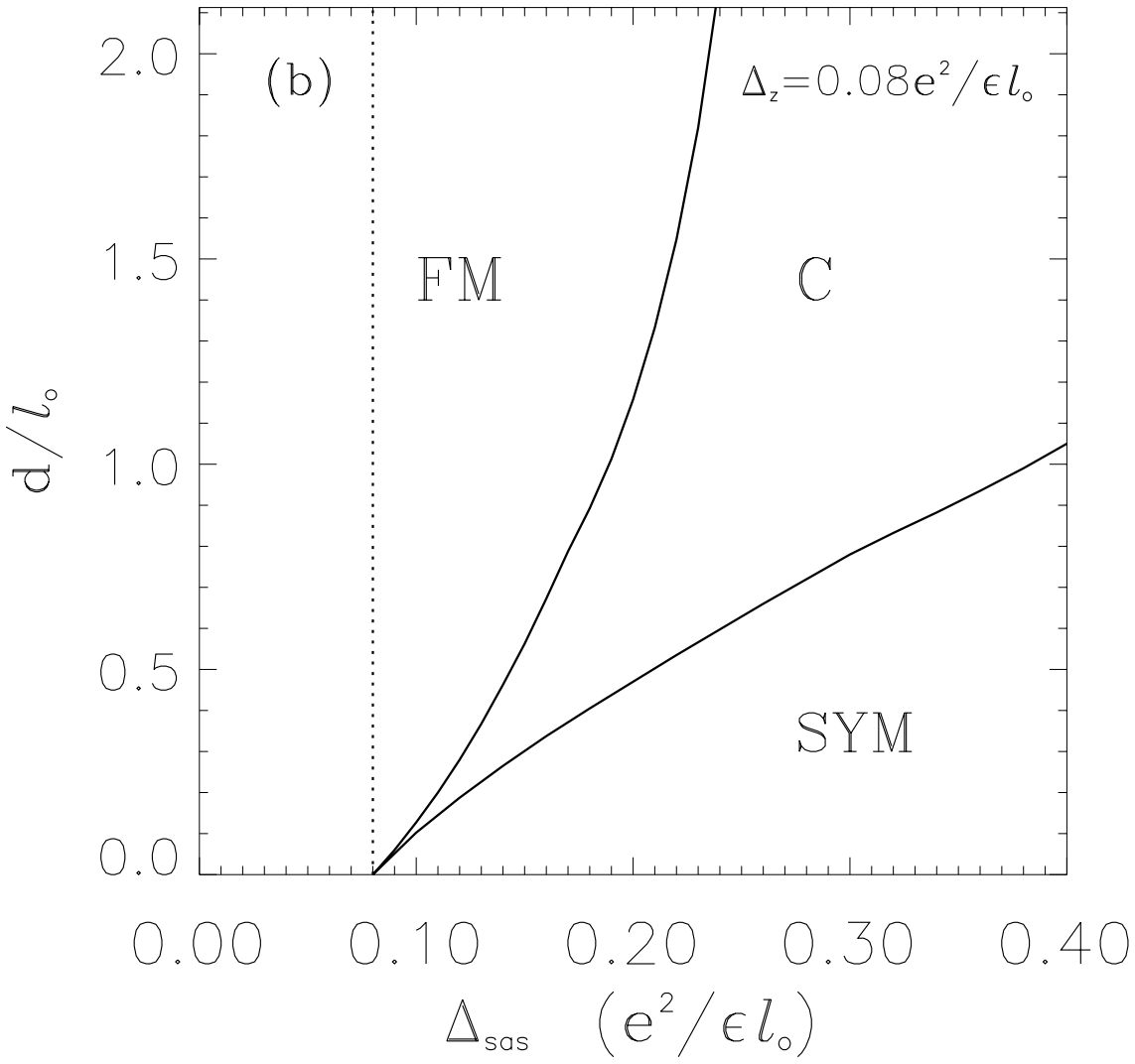

Fig 5 Zheng, Das Sarma, Sachdev

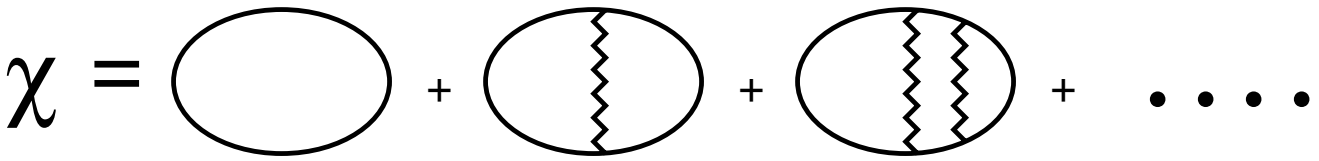

Fig6 Zheng, Das Sarma, Sachdev

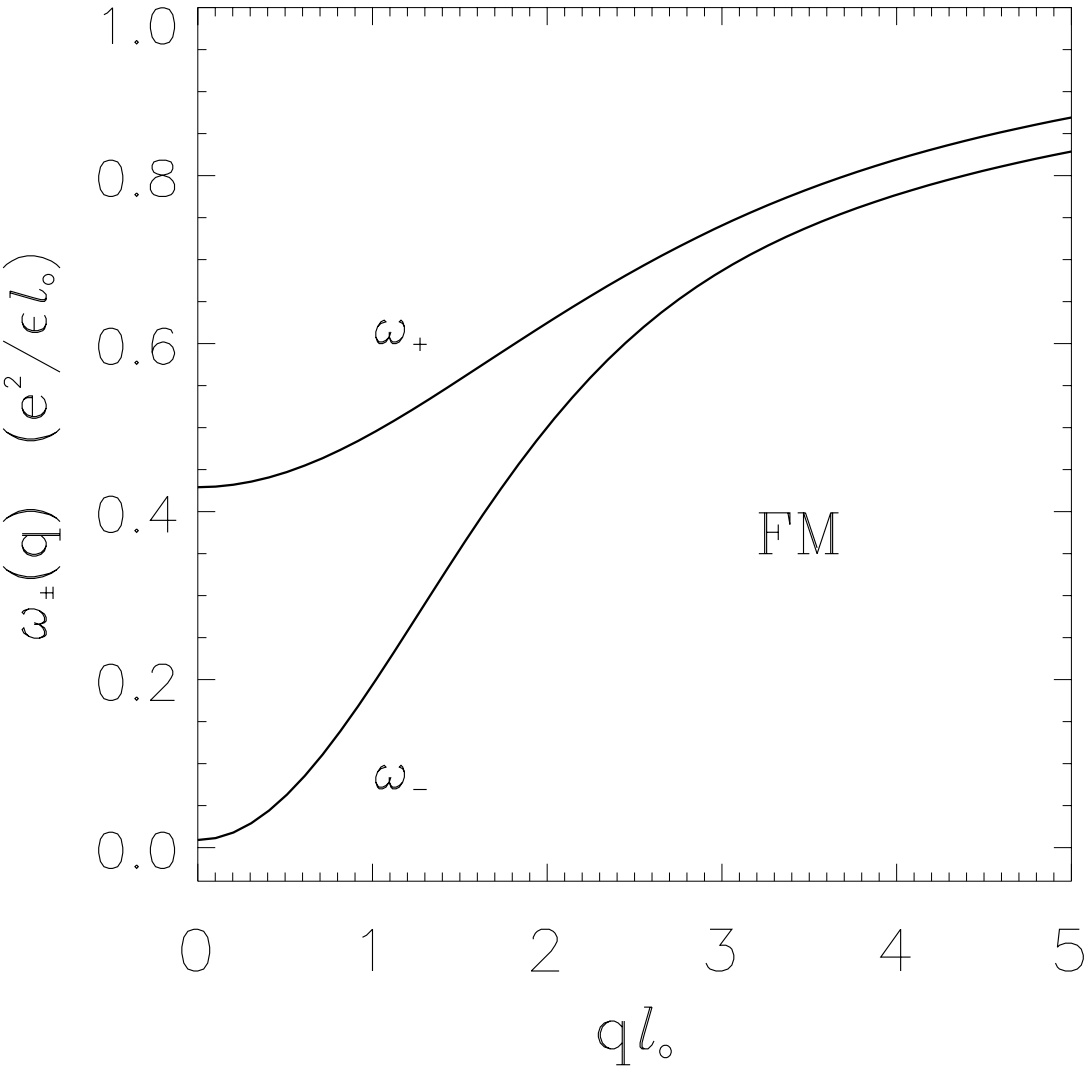

Fig7 Zheng, Das Sarma, Sachdev

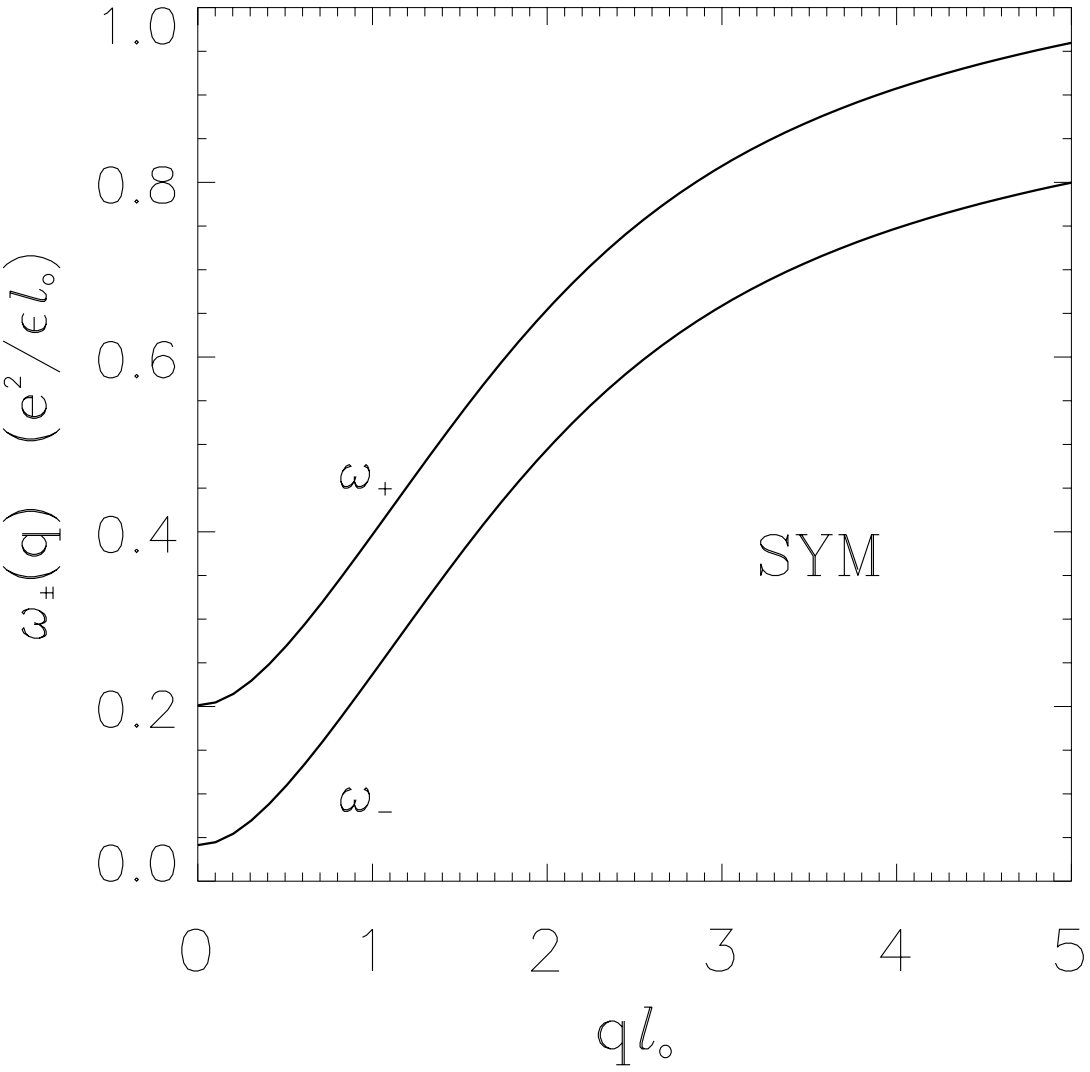

Fig8 Zheng, Das Sarma, Sachdev

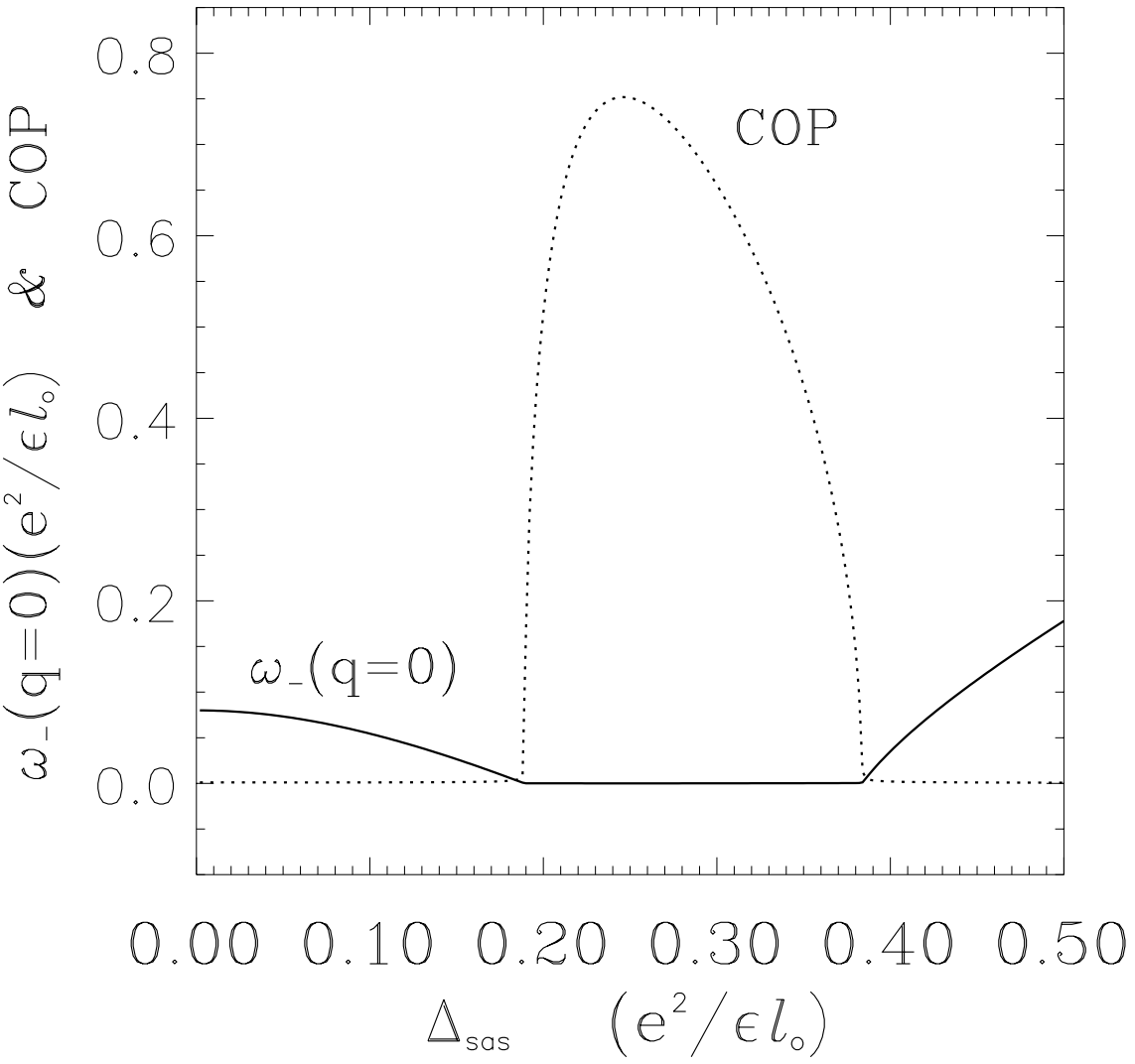

Fig9 Zheng, Das Sarma, Sachdev

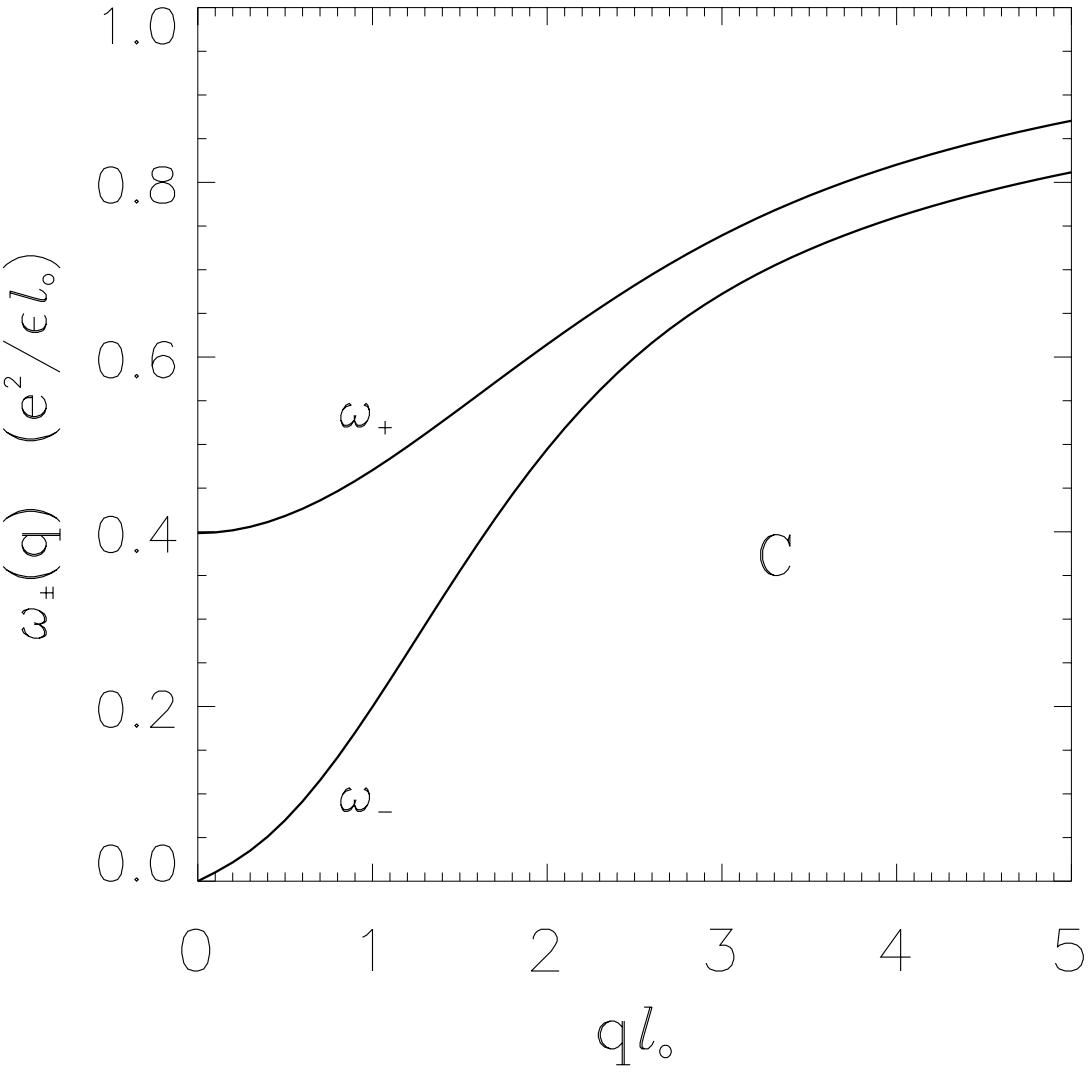

Fig.10 Zheng, Das Sarma, Sachdev

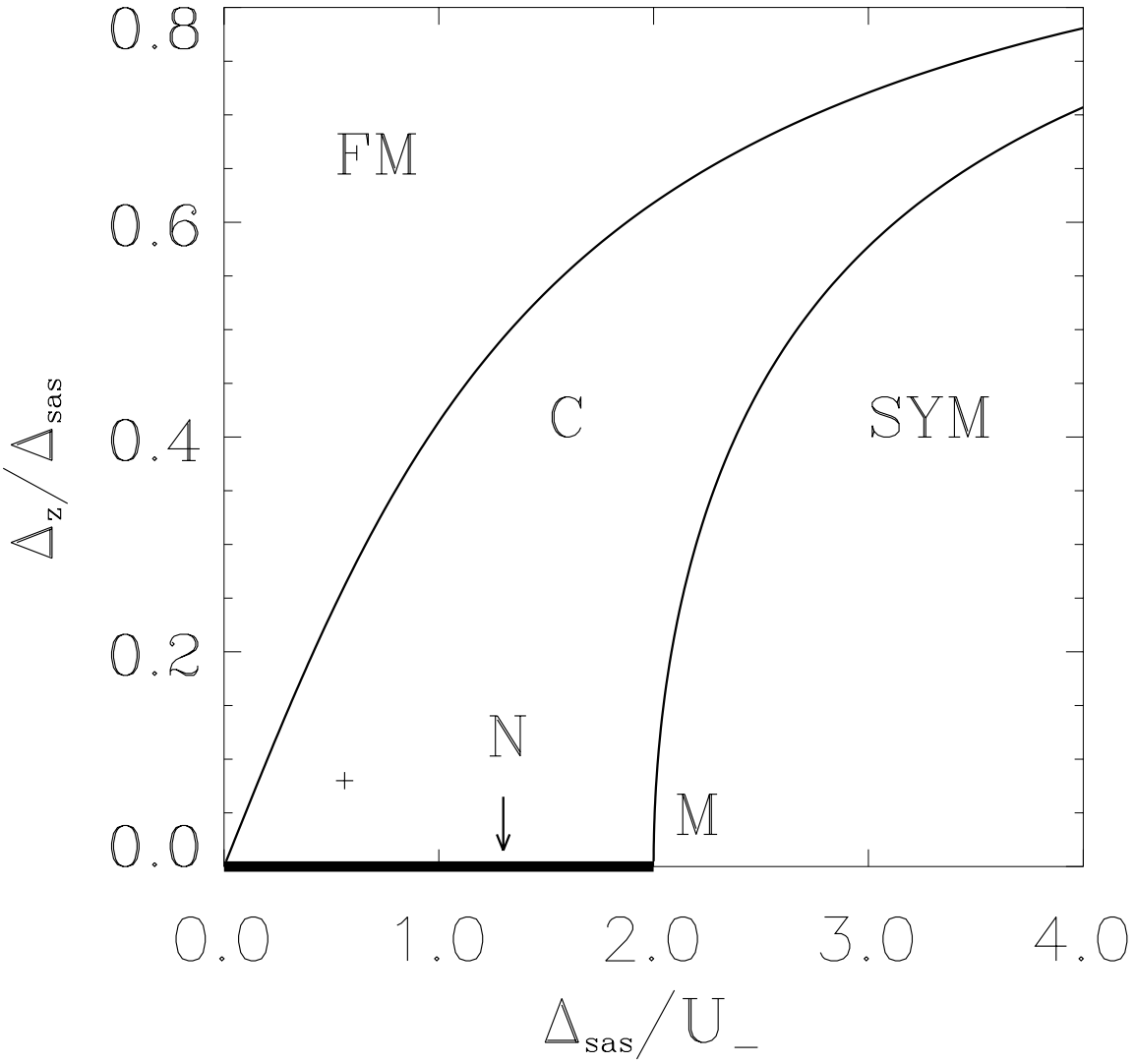

Fig11 Zheng, Das Sarma, Sachdev

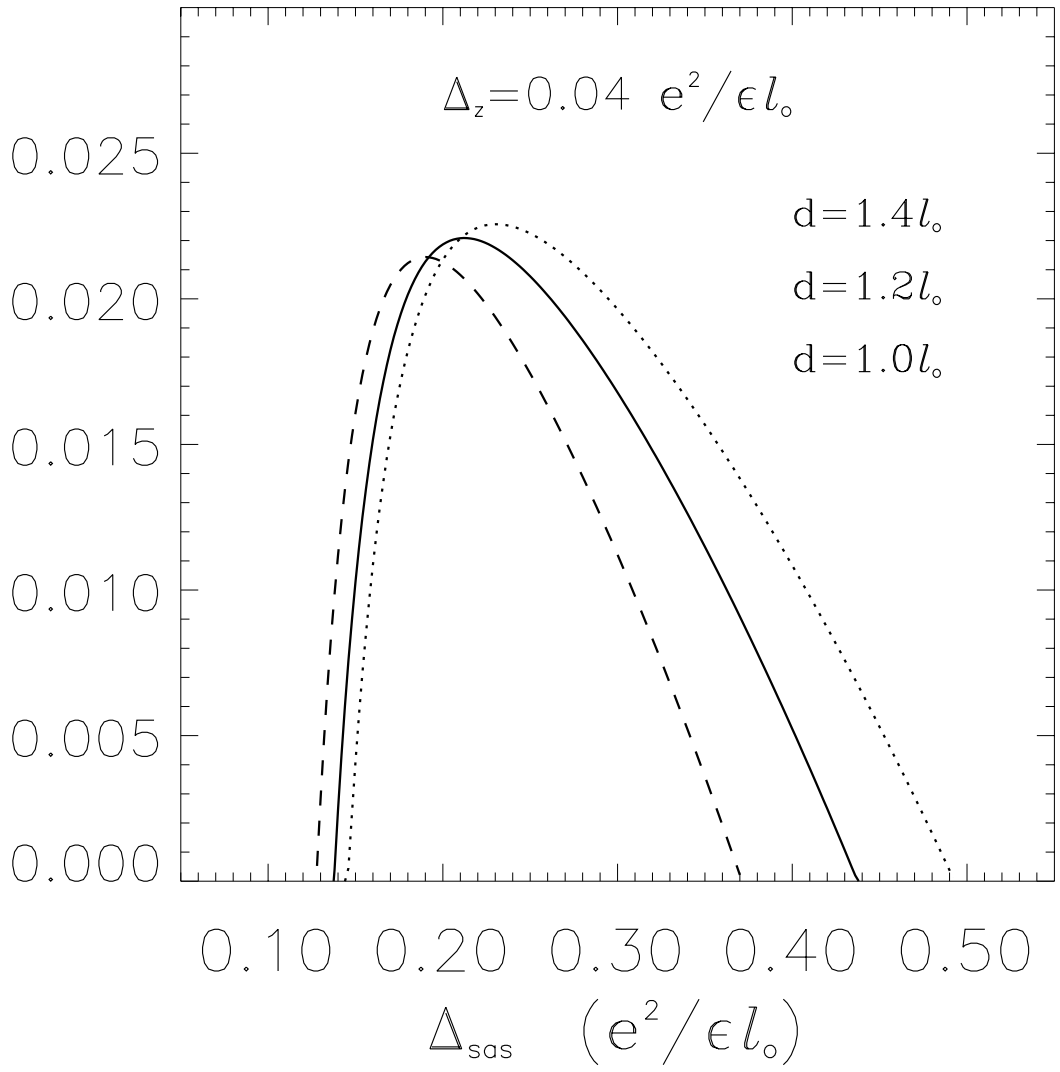

Fig12 Zheng, Das Sarma, Sachdev

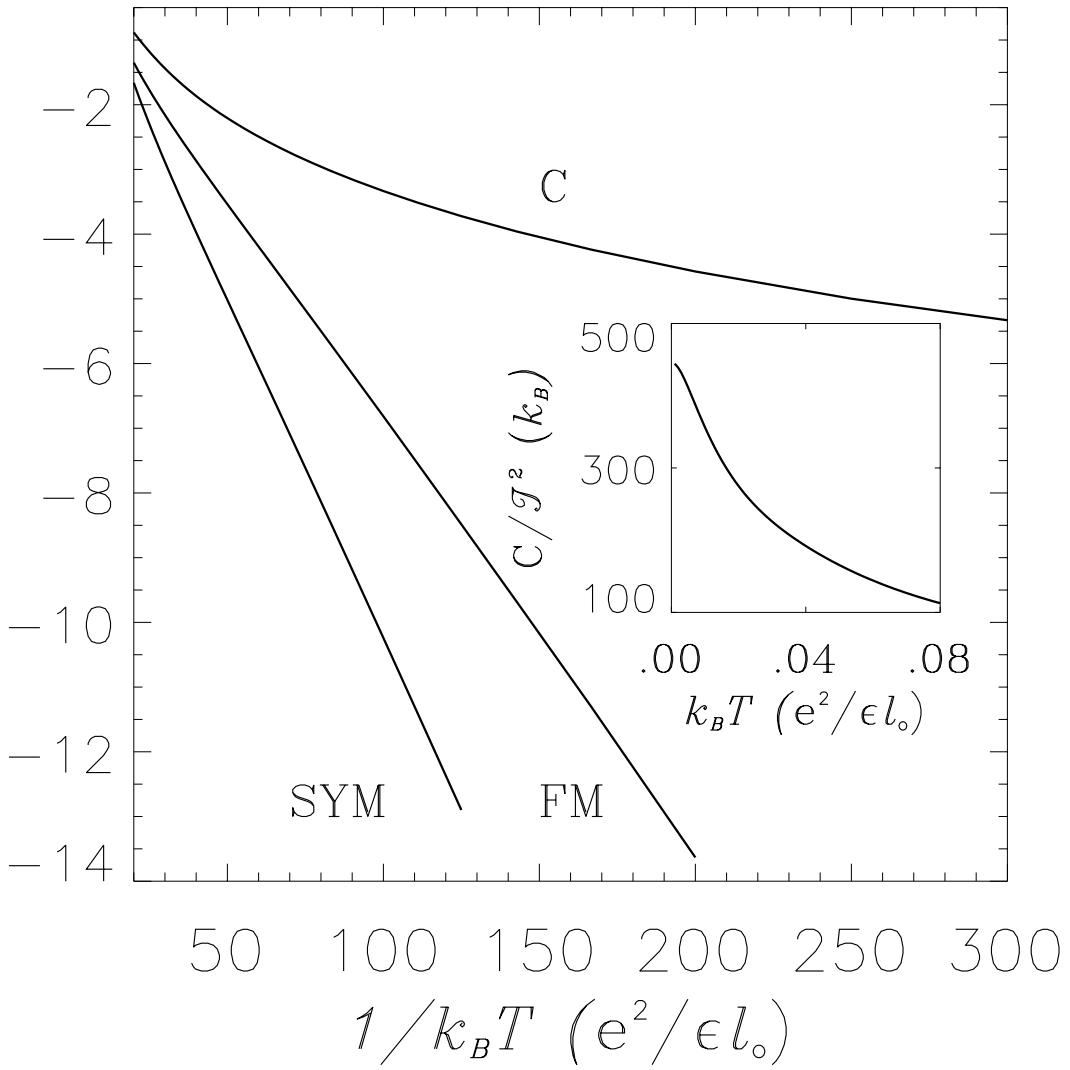

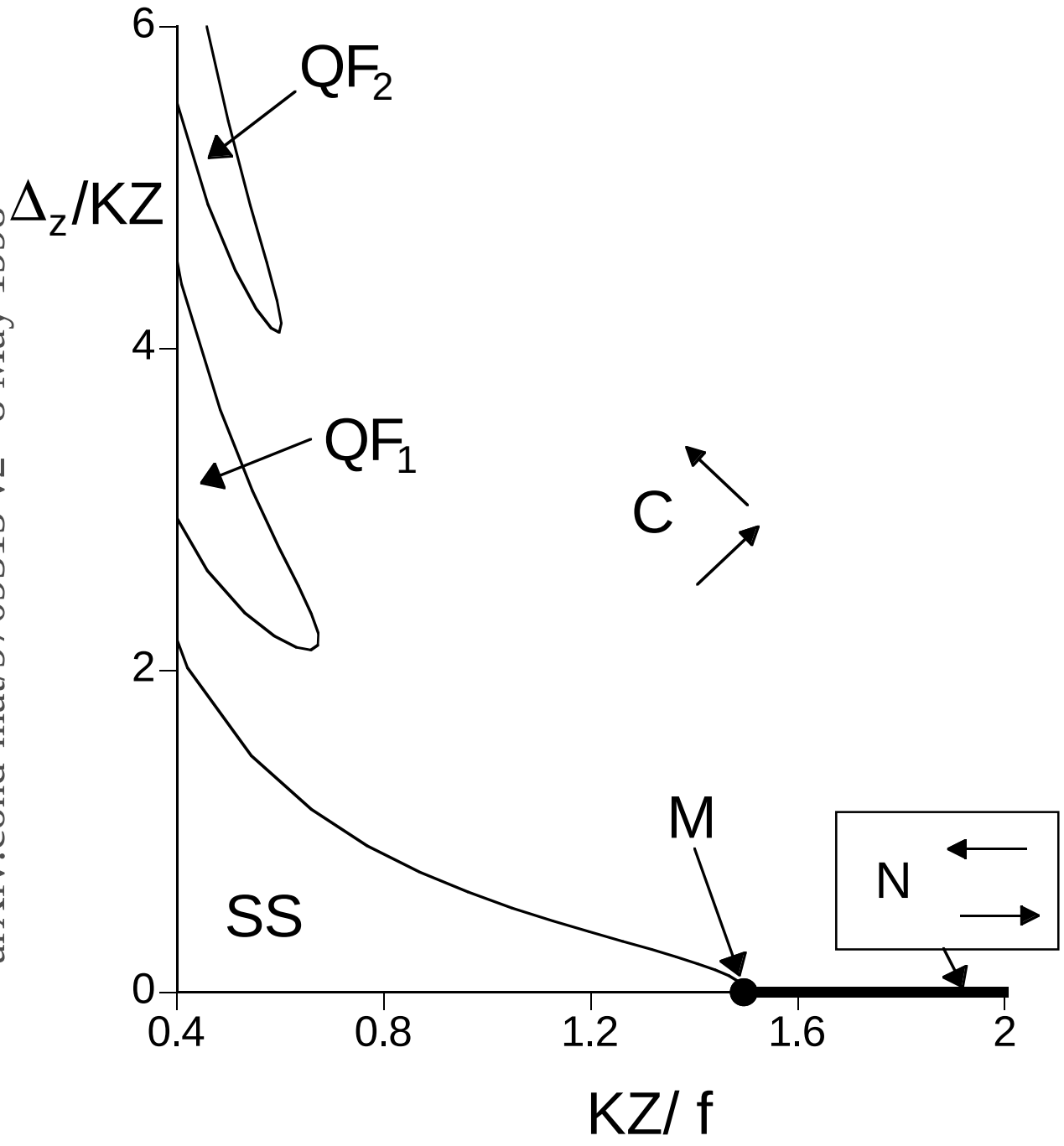

Fig 13 Zheng, Sachdev and Das Sarma

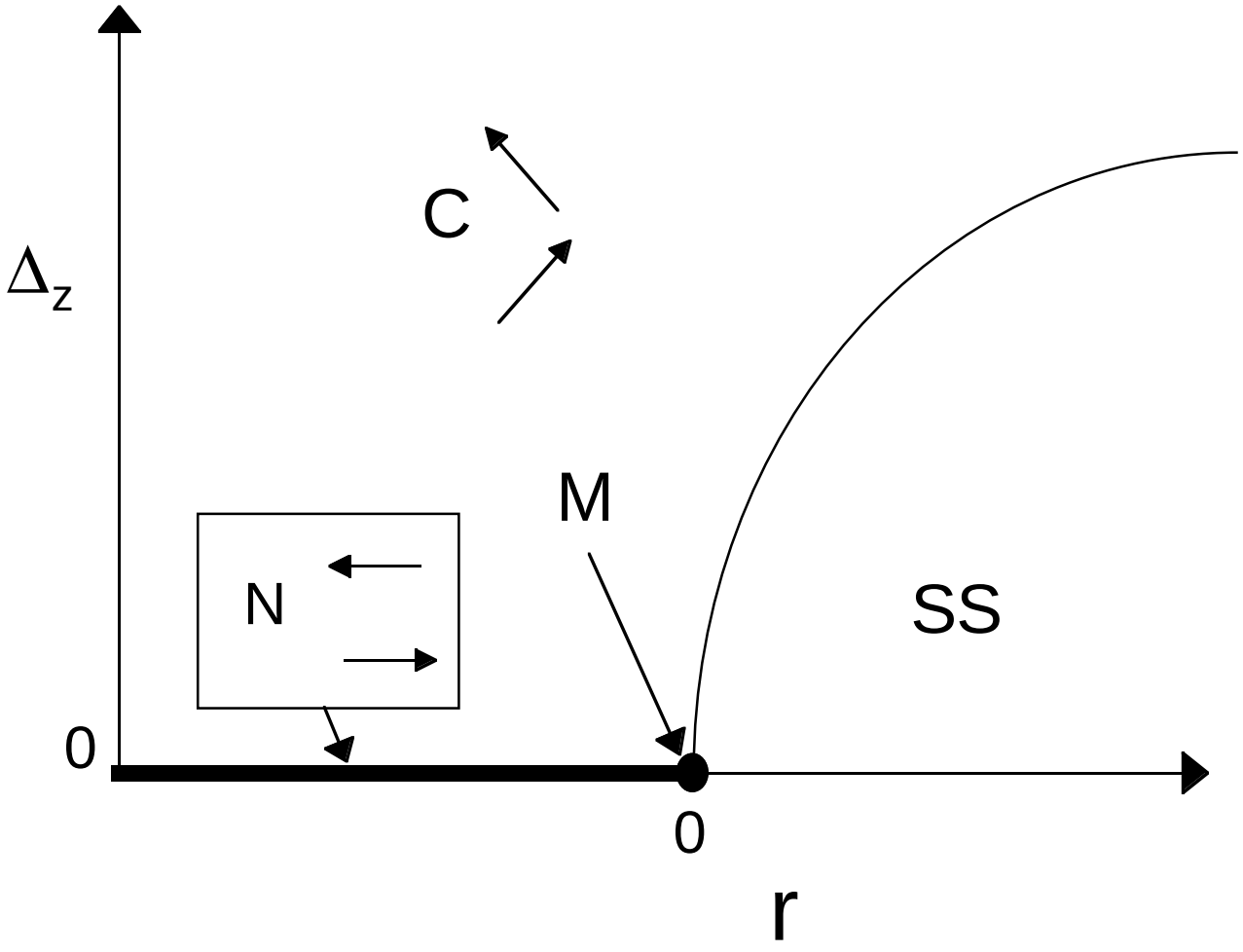

Fig 14 Zheng, Sachdev and Das Sarma

Fig. 15(a) Zheng, Das Sarma, Sachdev

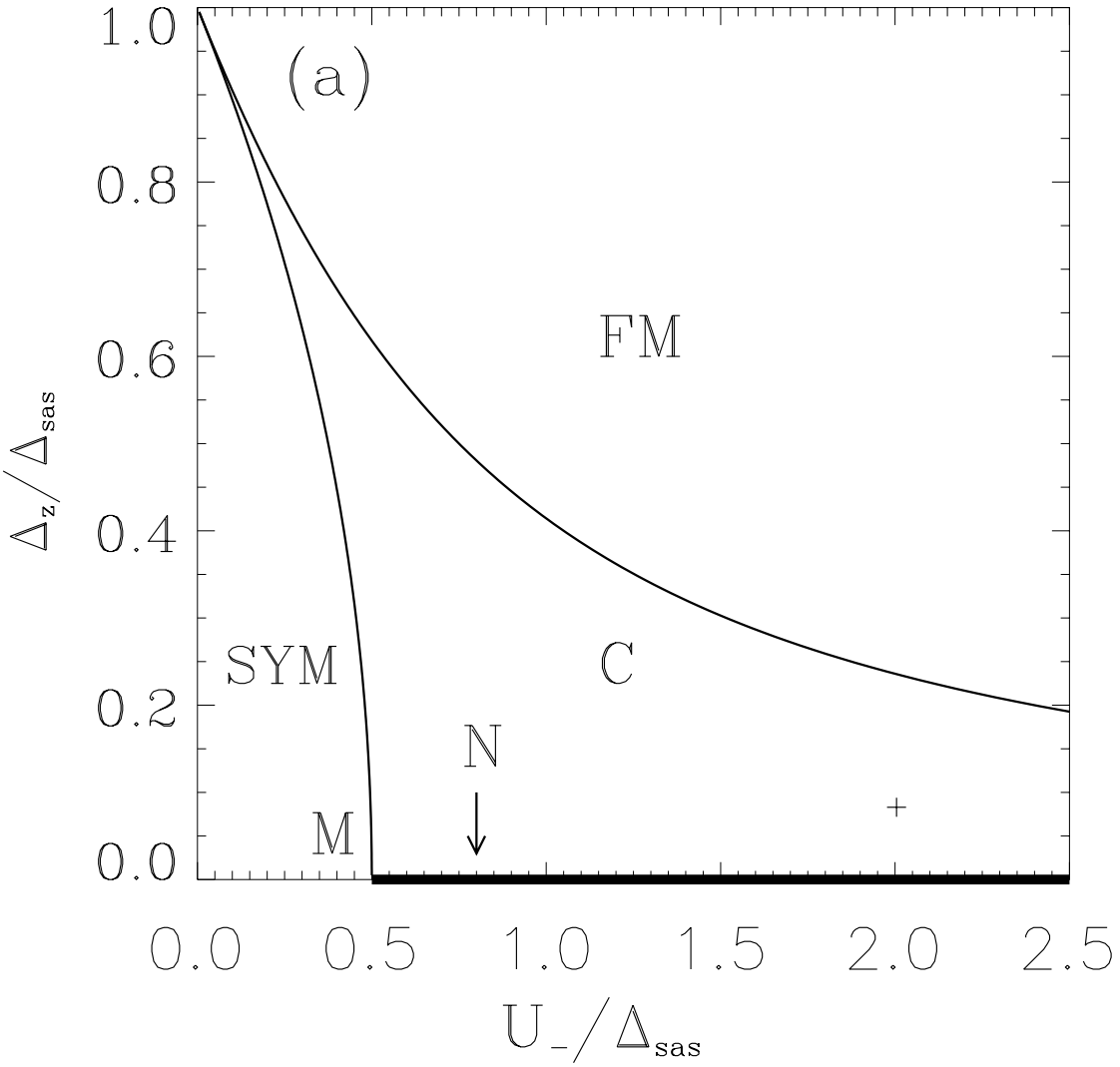

Fig. 15(b) Zheng, Das Sarma, Sachdev

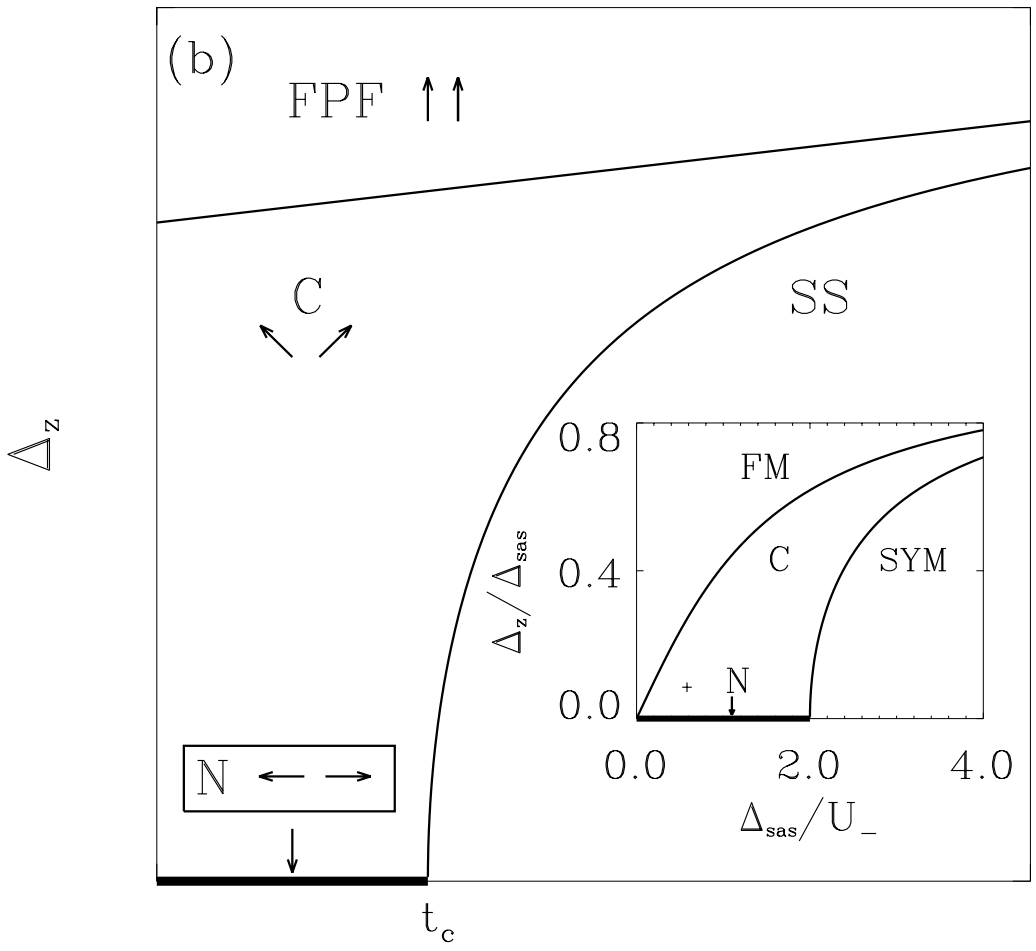

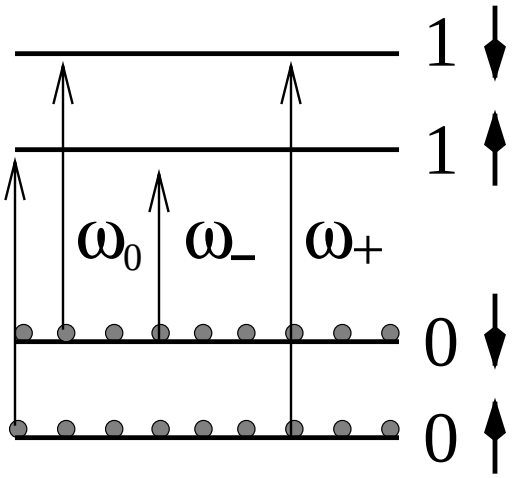

(a)

Fig 16(a) Zheng, Das Sarma, Sachdev

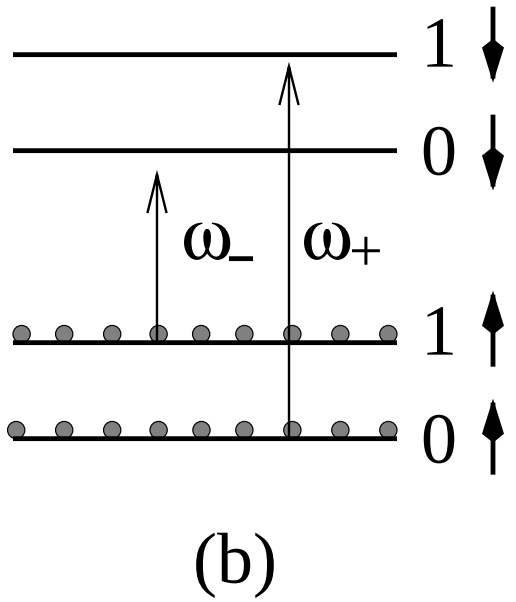

(b)

Fig. 16(b) Zheng, Das Sarma, Sachdev

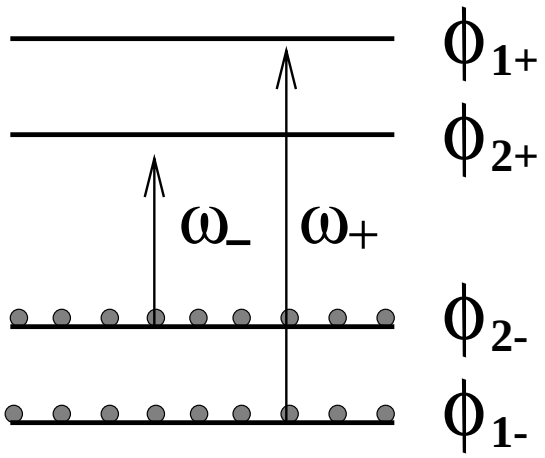

(c)

Fig. 16(c) Zheng, Das Sarma, Sachdev